HDL-TR-1976
November 1981

Target Classification for the Installation Security Radar System

by Richard T. Antony

U.S. Army Electronics Research and Development Command
Harry Diamond Laboratories
Adelphi, MD 20783

Approved for public release; distribution unlimited.

UNCLASSIFIED

SECURITY CLASSIFICATION OF THIS PAGE *(When Data Entered)*

REPORT DOCUMENTATION PAGE	READ INSTRUCTIONS BEFORE COMPLETING FORM
1. REPORT NUMBER: HDL-TR-1976	2. GOVT ACCESSION NO.: FID-A109473
3. RECIPIENT'S CATALOG NUMBER:	
4. TITLE *(and Subtitle)*: Target Classification for the Installation Security Radar System	5. TYPE OF REPORT & PERIOD COVERED: Technical Report
	6. PERFORMING ORG. REPORT NUMBER:
7. AUTHOR(s): Richard T. Antony	8. CONTRACT OR GRANT NUMBER(s): MIPR: FY7616780005
9. PERFORMING ORGANIZATION NAME AND ADDRESS: Harry Diamond Laboratories, 2800 Powder Mill Road, Adelphi, MD 20783	10. PROGRAM ELEMENT, PROJECT, TASK AREA & WORK UNIT NUMBERS: Program Ele.: 63305F MX Wide Area Surveillance System
11. CONTROLLING OFFICE NAME AND ADDRESS: MX Project Office, BHO/MNNBO (CPT R. Kravetz), Norton Air Force Base, CA 92409 and Headquarters ESD/OCB, Hanscom Air Force Base, Bedford, MA 01731	12. REPORT DATE: November 1981
	13. NUMBER OF PAGES: 60
	15. SECURITY CLASS. *(of this report)*: UNCLASSIFIED
	15a. DECLASSIFICATION/DOWNGRADING SCHEDULE:

16. DISTRIBUTION STATEMENT *(of this Report)*

Approved for public release; distribution unlimited.

17. DISTRIBUTION STATEMENT *(of the abstract entered in Block 20, if different from Report)*

18. SUPPLEMENTARY NOTES

HDL Project: 524852

19. KEY WORDS *(Continue on reverse side if necessary and identify by block number)*

Target classification
Target identification
Pattern recognition
Signature analysis

20. ABSTRACT *(Continue on reverse side if necessary and identify by block number)*

Target classification is discussed as applied to a ground-based site-security radar system. Discrimination functions were developed for human, vehicle, small animal, bird, and nontranslating return. Acceptable classification performance was achieved for single-cell assessment, and high-confidence classification is expected for multiple-cell (i.e., track) assessment.

DD FORM 1 JAN 73 1473 EDITION OF 1 NOV 65 IS OBSOLETE

UNCLASSIFIED

CONTENTS

Figures

Figures (Cont'd)

Figures (Cont'd)

Tables

1. INTRODUCTION

This paper discusses the use of pattern recognition to automatically assess targets detected by the Installation Security Radar (ISR) system.* The ISR is a uhf site-security radar with a 360-degree electronic step-scan capability. A coherent receiver develops both the in-phase and quadrature components of the Doppler return. Detection processing is implemented with a high-speed microprogrammable processor[1] for 1024 cells chosen from the available 8192 range-azimuth cells. Each cell is 11.5 degrees wide by 15 m deep. Target classification and track processing are initiated upon target detection.

Radar backscatter from a range-azimuth cell contains information about the scattering objects within that cell. Target classification as addressed in this paper uses this inherent information to assign priorities to possible threat-target tracks and to minimize the formation of tracks on nuisance targets, such as birds and animals, and false targets, such as foliage backscatter and system noise. Target classifiers have been designed and evaluated with a relatively large data base obtained jointly by Sandia Laboratories (SL) and the Harry Diamond Laboratories (HDL) at the Department of Energy's PANTEX facility in Texas. The data were obtained with a Camp Sentinel Radar (CSR)[2] driving digital recording hardware with software developed at SL.

2. PATTERN RECOGNITION APPROACH

Conceptually, pattern recognition involves the three operations of feature definition and ranking, feature extraction, and class discrimination. In this study the essential target features were determined as derived parameters of a simple radar-backscatter return model. The Doppler return is Fourier transformed, and the features are extracted in the spectral domain. Discriminant functions map regions of the N-dimensional feature subspace to regions of the M-dimensional decision space. In general, various classifier structures and optimality criteria are available for selecting the class discriminator. In this paper, class discrimination is based on the value of the conditional a posteriori probability functions evaluated at estimates of the spectral features.

**Concept Evaluation Phase of the Installation Security Radar System, HDL internal report, 24 December 1980 (available from author).*

[1]R. Lewis, PMP-2 Processor Handbook, Stein Associates, Inc., Waltham, MA (March 1978).

[2]J. Dent, Camp Sentinel Radar III (U), 18th Tri-Service Radar Symposium (1972). (CONFIDENTIAL)

Although numerous distance measures have been suggested for evaluating feature selection, Kanal[3] suggests that it is best to measure the probability of error directly. For the ISR, the a priori probability of each target class is not known. Therefore, instead of maximizing the total probability of error, the present target classifiers were developed by maximizing the probability of proper classification, while minimizing the probability of improper classification for each target class taken separately.

2.1 Target Models

The use of physical models to predict the spectral character of the Doppler return offers at least three benefits to the development of target classifiers. First, a physical model allows efficient use of the available data base since only the essence of the spectral characteristics of the return is used to develop the model and hence design the classifier. Typically, at least one-half of a data base is used during classifier training (e.g., to obtain the weights, for a linear classifier). Second, strategies to determine the "best" feature subset are not necessary, since the ranking of the spectral features occurs naturally from the development of the target model. Third, the use of target modeling yields an intuitive relationship between the spectral features and such physical parameters as target velocity, direction of travel relative to radial, step size, and step rate. Because of the structure present in the data, this type of target modeling (as opposed to less intuitively motivated methods such as principal-component modeling) seems to be well suited to the problem.

2.1.1 Translating Targets

A simple three-point target-backscatter model possesses the essential spectral character of the uhf return from a translating target. The modelled return, V, is the vector sum of the contributions from the target body and its moving appendages:

$$V = \sum_{i=1}^{3} a_i(t) \cos \frac{4\pi r_i(t)}{\lambda} \quad . \tag{1}$$

The $a_i(t)$ ($i = 1, 2, 3$) represent the variation in cross section of the i^{th} scattering point as a function of time; $r_i(t)$ ($i = 1, 2, 3$) represent the distance between the i^{th} scattering point and the radar as a function of time; and λ is the rf wavelength.

---

[3] *L. Kanal, Patterns in Pattern Recognition: 1968-1974, IEEE Trans. Inf. Theory, IT-20, 6 (November 1974), 697-722.*

If the first reflector represents the return from the torso, $r_1(t)$ is a monotonic function of time. The second and third reflectors then represent the return from the moving appendages (e.g., human arms and legs, bird wings) and thus $r_2(t)$ and $r_3(t)$ possess both a monotonic and an oscillatory component. The return from a wheeled vehicle can be considered a degenerate case with only a single scattering point. For constant-velocity targets, V can be expressed as

$$V = a_1(t) \cos\left(2\pi f_T t\right) + a_2(t) \cos\left[2\pi f_T t + \phi_1(t)\right] + a_3(t) \cos\left[2\pi f_T t + \phi_2(t)\right] , \quad (2)$$

where

$$f_T = \frac{2V_R}{\lambda} \cos \gamma$$

V_R = target radial velocity,

γ = angle of target travel relative to radial, and

$\phi_1(t)$ and $\phi_2(t)$ are angle modulation terms caused by the moving (resonant) appendages.

The periods of $a_i(t)$ ($i = 1, 2, 3$) and $\phi_j(t)$ ($j = 1, 2$) are related to the appendage resonant frequency (or target natural frequency, f_0).

Assuming that $\phi_1(t) = \phi_2(t) + \pi$ and $a_2(t) = a_3\left(t + 1/f_0\right)$, equation (2) can be written in the simplified form:

$$a_1(t) \cos\left(2\pi f_T t\right) + 2a_2(t) \cos\left[2\pi f_T t + \phi_1(t)\right] . \quad (3)$$

A sample of the measured power spectral density function from a radially inbound human is shown in figure 1. Figure 2 shows an example of the power spectral density function of a synthetically generated target signal based on equation (3). The modelled human-target return (fig. 2) can be seen to possess much of the same spectral character as the real radar return.

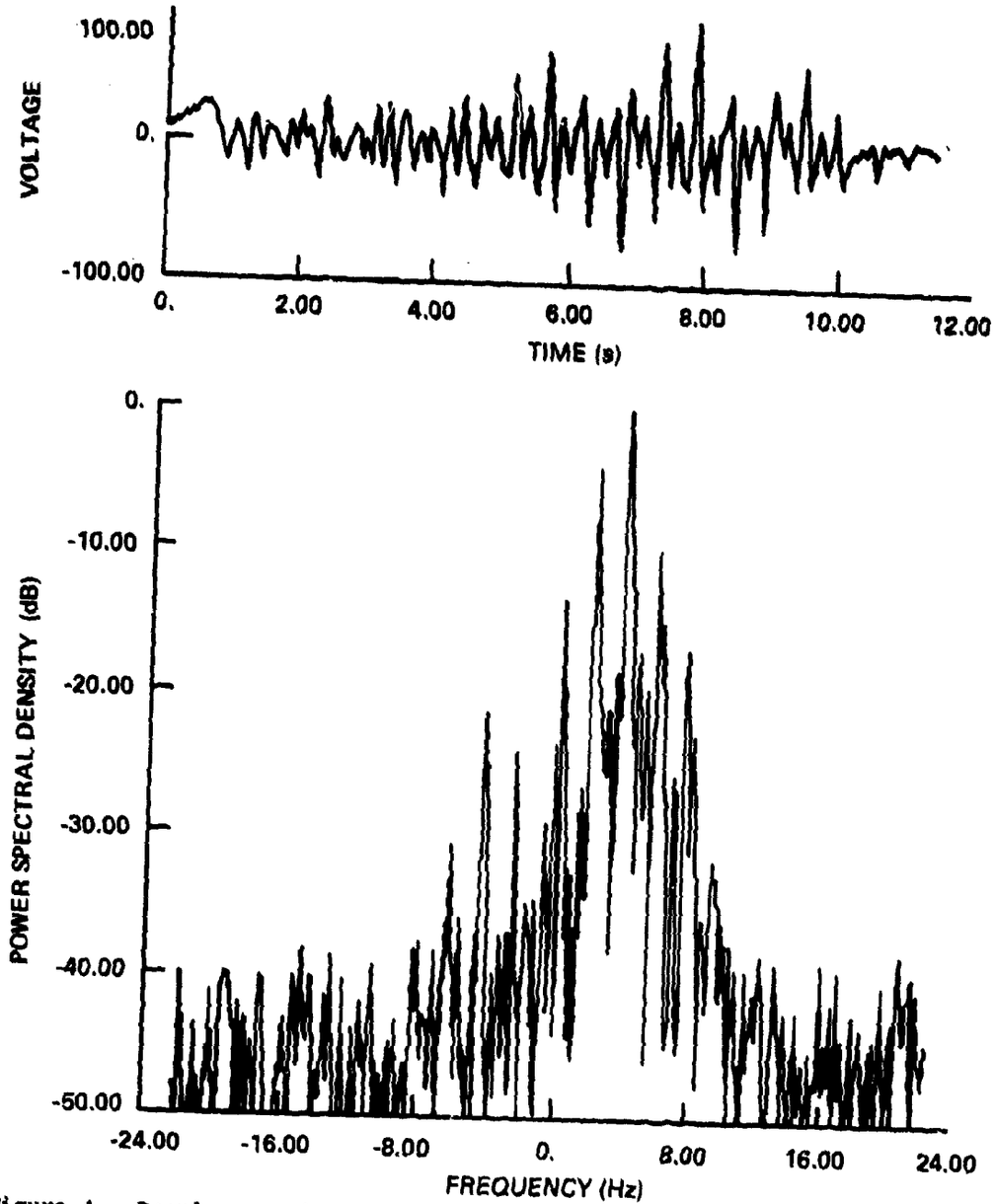

Figure 1. Doppler waveform and power spectral density function of return from a human target walking radially in-bound, at a step rate of 100 steps per minute with normal arm and leg motion.

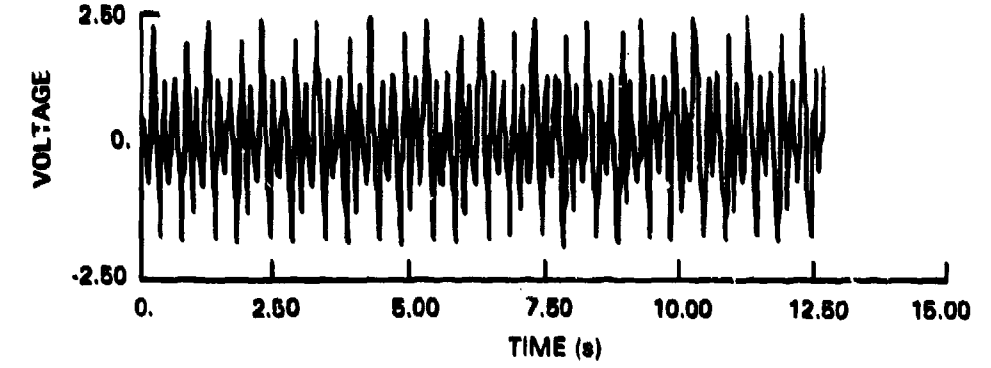

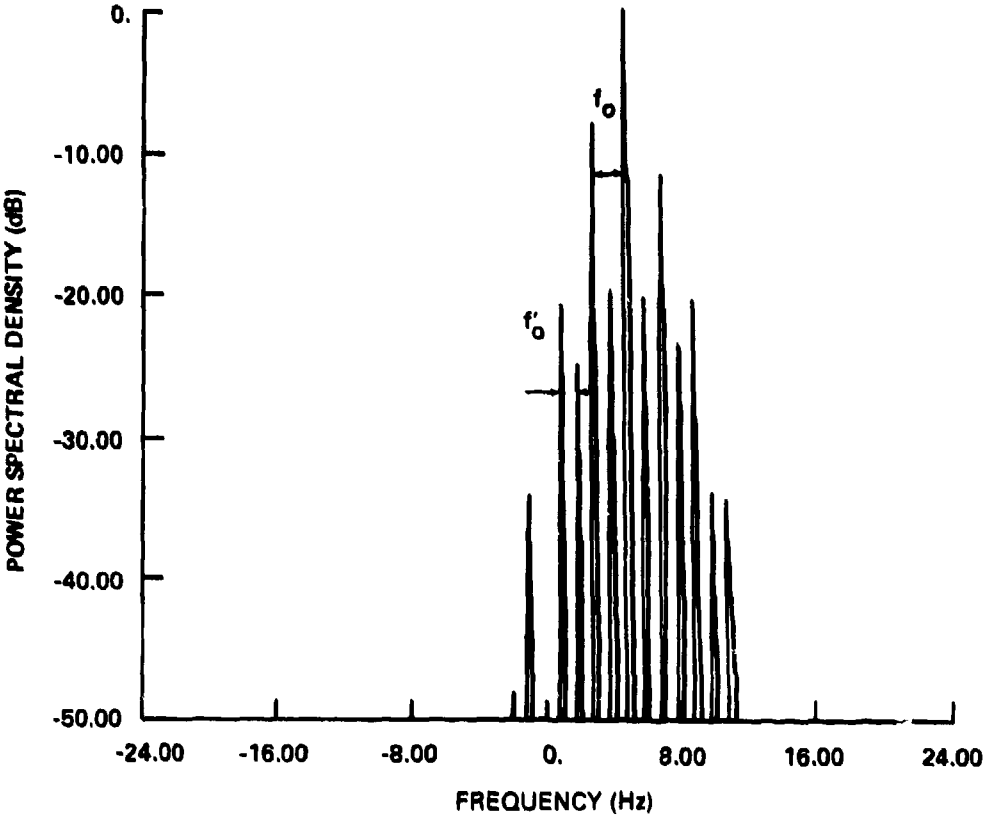

Figure 2. Typical Doppler waveform (no range cell weighting) and power spectral density function generated by generalized target model (eq (3)).

Human return.--The important target attributes that appear to be obtainable from the Doppler return are (1) target velocity, (2) target natural frequency, (3) distance traveled in one cycle of limb motion, (4) limb modulation characteristics, (5) indication of target mass, and (6) relative size of the target. Some of these attributes can be estimated directly from the spectrum of the target return, while others must be indirectly estimated. Because of shadowing, roughness, multipath effects, the target's height above ground, etc, the estimate of relative target size may be in error by more than an order of magnitude. For this reason, only the first five attributes will be considered:

(1) f_T is related to the target radial velocity, V_R; i.e,

$$f_T = \frac{2V_R}{\lambda} \quad .$$

Of considerably more interest is the actual target velocity, V_T, and not just its radial component; i.e.,

$$V_T = V_R \sec \gamma \quad ,$$

where γ is typically unknown. A possible means of estimating γ is given shortly. The highest velocity for a sprinting human is approximately 30 ft/s while a dog's velocity can be twice that high. Thus, although a measured velocity of greater than 30 ft/s does not inevitably imply a dog target, it rules out the possibility that the return is due to a human.

(2) f_0 is the natural frequency of the target. In the case of a human, f_0 is equal to one half the step rate, while for a bird it is equal to the wing-beat frequency. The highest expected natural frequency for a human is approximately 5 Hz, while a duck and a sparrow have natural frequencies of approximately 9 and 13 Hz, respectively. Although large birds have wing-beat rates on the order of a human's natural frequency, most birds have significantly higher natural frequencies. In the case of nonnatural targets such as helicopters, the propeller rotation rate is significantly higher than most bird wing-beat rates.

(3) f_T/f_0 is proportional to the distance of radial target travel in one cycle of the target's natural frequency. This distance measure is given by d_0, where

$$d_0 = \frac{\lambda}{2} \frac{f_T}{f_0} \sec \gamma \quad .$$

In the case of a human, d_0 represents the target step size. An estimate of γ is required to fully use the quantity f_T/f_0.

(4) The nature of the limb modulation is expected to be a species-dependent characteristic. In addition, it has been empirically observed that by comparing the relative power in the limb modulation and torso return for natural targets, an indication of the angle of target travel relative to radial may be obtained. This phenomenon has not been fully explained but may be due to masking of or interference among the dominant scatterers.

For a human on a radial trajectory, the translation lobe in the spectral return is somewhat larger than the modulation sidelobes. As the angle relative to radial increases, the power in the translational lobe relative to the power in the modulation harmonics diminishes for an outbound target and increases for an inbound target, as shown in figures 3 and 4, respectively. By using such information, an estimate can perhaps be made of the direction of target travel relative to radial. An estimate of γ could be used by both the tracking function for trajectory prediction and in the calculation of target step size.

(5) The spectral width of the translational component and modulation sidelobes of the target return may provide additional target discrimination. As suggested by L. T. James (SL) and R. Chase (HDL), this spectral width contains information about acceleration of the target and its appendages. In certain cases the spectral width may be related to the mass of the target.

For an upright walking human, the spectral width of the target translational component, Δf_T, generally increases with increasing target velocity. If Δf_T is written as some function, $g()$, of the target velocity, V_T, then

$$\Delta f_T = g\left(\frac{\lambda}{2}\,\frac{f_T}{\cos\,\gamma}\right). \tag{4}$$

Assuming that the inverse of g exists (i.e., $g^{-1}()$), then an estimate of γ can be obtained as

$$\hat{\gamma} = \cos^{-1}\left[\frac{\lambda}{2}\,\frac{f_T}{g^{-1}(\Delta f_T)}\right]. \tag{5}$$

Similarly, since $d_0 = (\lambda/2)(f_T/f_0)\sec\gamma$, if $g^{-1}()$ exists, d_0 can be expressed as

$$d_0 = \frac{g^{-1}(\Delta f_T)}{f_0} \quad . \tag{6}$$

Once the function g and its inverse are obtained, the estimates of γ and d_0 depend only on the easily measured spectral attributes f_T, f_0, and Δf_T. The two separate estimates of γ were made based on (1) the power in the translational component relative to the modulation sidelobes and (2) the relative width of the translational component. These single-cell estimates of γ can be correlated with the observed target trajectory over multiple cells to produce an accurate estimate of angle of target travel relative to radial.

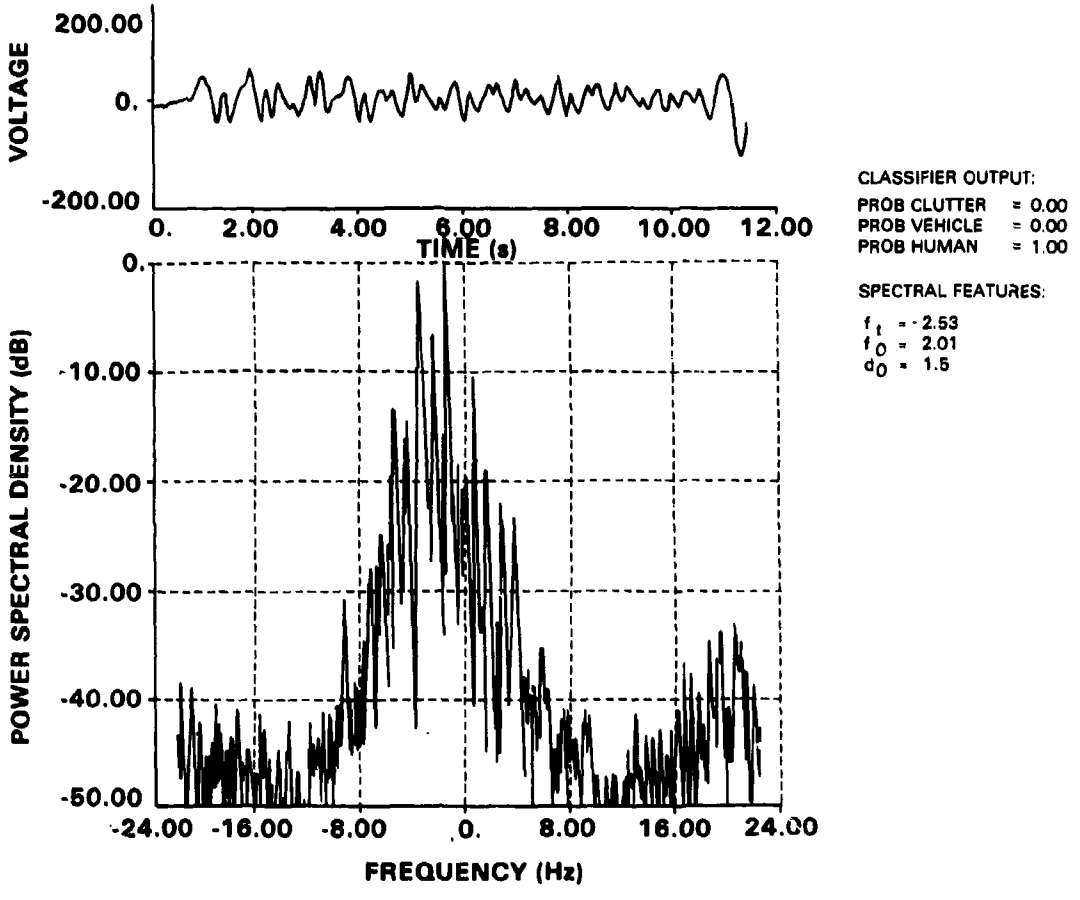

Figure 3. UHF return from an outbound human, traveling at an angle of 45° relative to radial, with a step size of 2 ft and step rate of 2 steps per second.

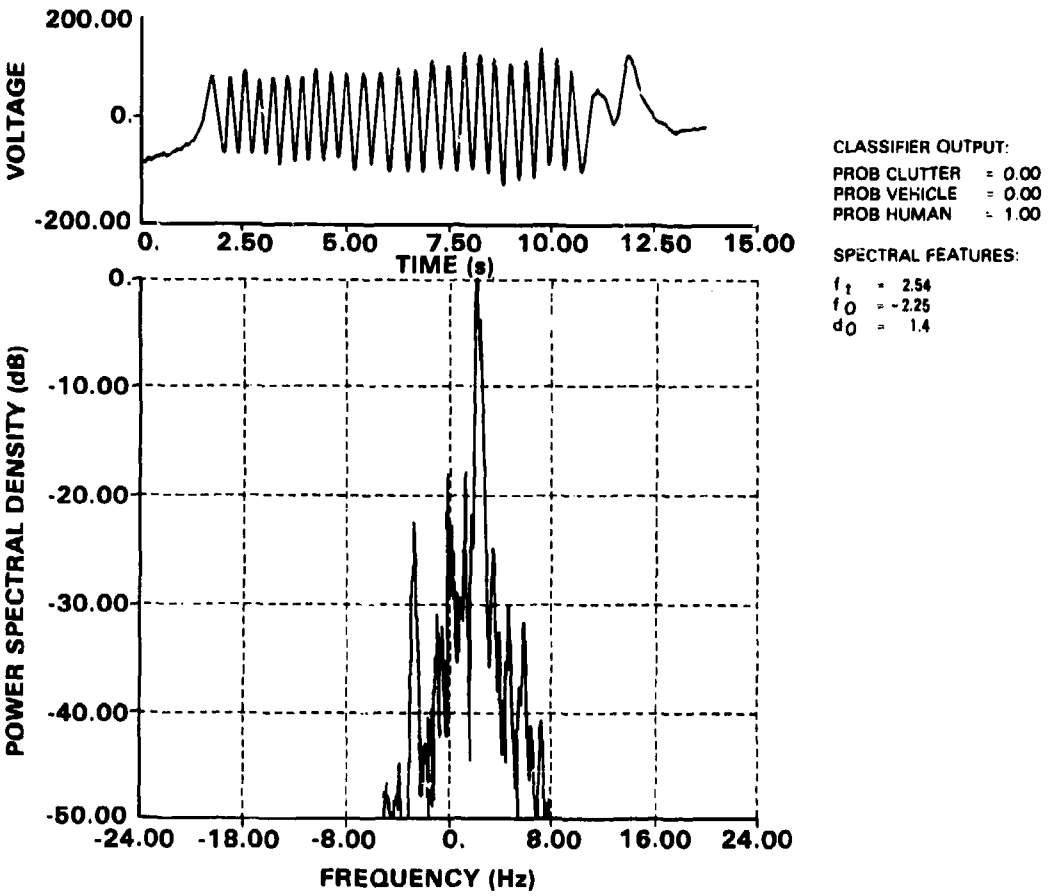

Figure 4. UHF return from an inbound human, traveling at an angle of 45° relative to radial, with a step size of 2 ft and step rate of 2 steps per second.

Bird return.--Birds can be expected to present a problem to a ground-based radar designed to detect humans and vehicles. The energy arriving at a target and that scattered back to the radar consists of both a direct path and a ground-reflected wave. A vertical lobe structure in the radiation pattern results from the interference phenomenon, as discussed by Skolnik.[4] The observable effect is that the radar return from a target near the ground falls off as the inverse of range to the eighth power, instead of the inverse of range to the fourth power, as with a target in free space.

[4] *M. Skolnik, Introduction to Radar Systems, McGraw-Hill (1980), Ch 12.*

For path length differences that are small compared to a wavelength, it is shown in appendix A that the received power from a target is proportional to

$$\frac{h_a^4(h_a + h_t)^4}{R^8} ,$$

where

h_a is the antenna height,

h_t is the target height, and

R is the (direct path) range to the target.

A plot of the approximate variation in radar return power expected from a point target as a function of target height is shown in figure 5. For example, with a 100-ft high radar antenna, the return from a target on the ground would be approximately 12 dB less than for the same target at a height of 100 ft.

A considerable amount of work has been reported in the literature on radar return from bird targets. Birds with physical extent somewhat less than one-half of the rf wavelength appear as Rayleigh scatterers with cross sections exhibiting a λ^{-4} wavelength dependence. At wavelengths less than the target extent, the cross section is expected to be proportional to the wavelength.[5] At approximately 3 GHz, the cross section of all birds, regardless of size, exhibits minimum spread (resonance).[5] Figure 6 compares the mean cross section of a human to that of several birds in the range of 0.4 to 10 GHz. Table 1 lists available average cross-section measurements at uhf (approximately 400 MHz) for several species of birds. Most sources suggest that the amplitude of the bird return follows a lognormal probability density function.[6] Cross-section measurements of birds in flight performed simultaneously at uhf, S, and X band have shown the standard deviation of the return to be of the same order of magnitude as the mean of the return.[6]

The most important discriminant reported in bird return is an amplitude modulation whose fundamental, f_0, is the wing-beat

[5] G. Pollon, *Distribution of Radar Angels, IEEE Trans. Aerosp. Electron. Syst.*, AFS-8, 6 (November 1972), 721-727.

[6] D. Atlas and K. Hardy, *Radar Analysis of the Clear Atmosphere: Angels, Progress in Radio Science 1963-66, International Scientific Radio Union, 15th General Assembly, Munich (5-15 September 1966).*

frequency.[7,8] This wing-beat frequency varies approximately inversely to the size of the bird;[9] this has been observed at frequencies from vhf to X band. Table 2 gives two suggested models for determining the characteristic wing-beat rate based on the bird wing length.

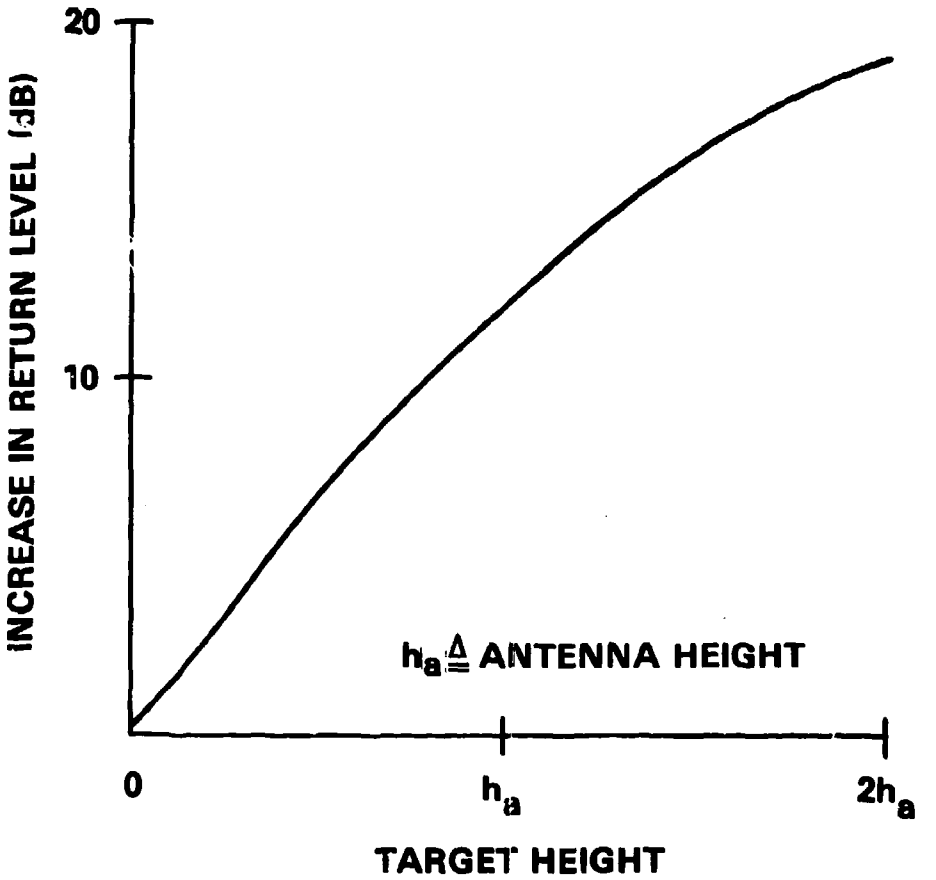

Figure 5. Approximate signal level increase (relative to return at zero height) as a function of target height above ground.

---

[7] *E. Reedy and T. Cutler, The HOWLS Radar Sky-Clutter Environment, Engineering Experiment Station, Georgia Institute of Technology, ESD-TR-75-319 (15 September 1975).*

[8] *W. Flock and J. Green, The Detection and Identification of Birds in Flight, Using Coherent and Noncoherent Radars, Proc. IEEE, 62, 6 (June 1974), 745-753.*

[9] *T. Konrad, J. Hicks, and E. Dobson, Radar Characteristics of Birds in Flight, Science, 159, 3812 (January 1968), 274-280.*

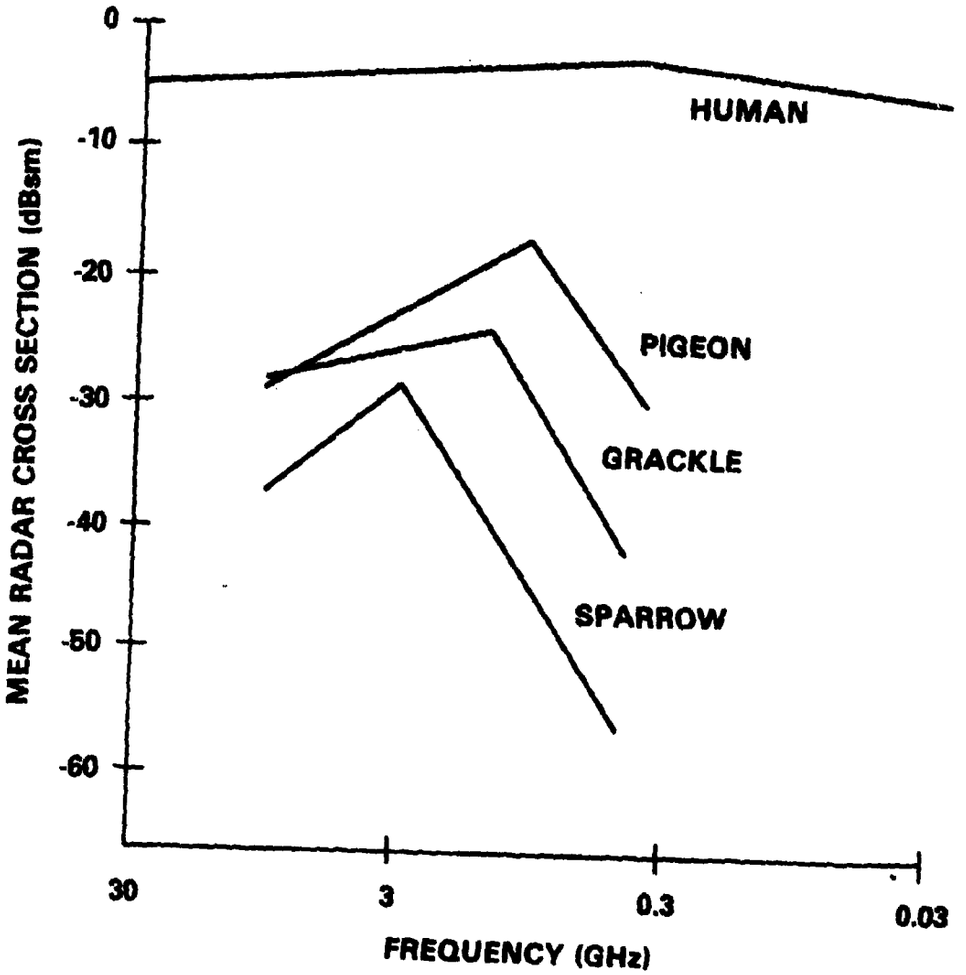

Figure 6. Examples of radar cross section of birds (excerpted from ref 7).

Wing-beat frequencies of between 11 and 15 beats per second were measured for a number of flights of a small pheasant at the PANTEX facility. The results agree reasonably well with the published results for comparable-size birds shown in table 3.

TABLE 1. UHF BIRD RADAR CROSS SECTION (ref 7)

Target	Radar cross section (dBsm)	Source
Pigeon	-30	Technology Service Corp.[a]
	-32	Condon[b]
Grackle	-42	Technology Service Corp.
	-44	Condon
Sparrow	-55	Technology Service Corp.
	-57	Technology Service Corp.

[a] *A Clutter Model for Artillery and Mortar Locating Radar, Technology Service Corp., TSC-PD-041-1, prepared for Mitre Corp. and USAECOM (7 July 1969).*

[b] *E. J. Condon, Scientific Study of Unidentified Flying Objects, New York Times, Bantam Books (1968), 655-716.*

TABLE 2. SUGGESTED MODELS RELATING WING LENGTH AND CHARACTERISTIC WING-BEAT RATE (ref 9)

Model[a]	Source
$f_0 \ell 1.15 = 3540$	Greenewalt[b]
$f_0 \ell 9.827 = 572$	Houghton[c]

[a] *f_0 is the wingbeat rate (Hz) and ℓ is the length of the wing (cm).*

[b] *C. H. Greenewalt, Hummingbirds, Doubleday and Co., Inc., Garden City, NY (1960).*

[c] *E. W. Houghton, The Effect of Changes in Target Trajectory on the Wingbeat Modulation Pattern, Royal Radar Establishment, RRE Memorandum No. 2456, Malvern, Worcs., England (1969).*

Since individual birds or flocks of birds could present serious false-alarm problems to a security radar system (especially at times of high activity such as the early morning, late evening, and migration seasons), considerably more backscatter return from bird targets needs to be obtained and analyzed in the future. Depending on the size of the bird and whether it is taking off, landing, flying level, or soaring, various wing-beat rates can be expected. Birds generally change direction more often and have a higher translational velocity (fig. 7) and a higher natural frequency (table 3) than a human target; thus, by monitoring the change in f_T, f_0, and f_T/f_0 along a target trajectory (through one or more range-azimuth cells), reliable algorithms can perhaps be developed to classify those tracks caused by birds.

TABLE 3. TYPICAL WING-BEAT RATES (ref 7)

Species	Rate (beats/s)
Sparrow	13
Duck	9
Crow	3 to 4
Stork	2
Pelican	1.1
Hummingbird	10 to 80

Animal return.--Target models similar to the human-target model need to be developed for each animal species that is expected to cause nuisance alarms at a given radar site. Since the uhf return from a biped can apparently be adequately modelled as an angle-modulated return with varying intensity depending on the step rate, quadrupeds should produce an intensity and angle modulation with a fundamental that corresponds to one-half or one-fourth the animal's step rate.

Vehicle and aircraft return.--Wheeled vehicles such as cars and small trucks appear to give an essentially monotone return, whereas tracked vehicles may produce return that contains certain modulation harmonics. Helicopters and propeller-driven aircraft are expected to produce return with modulation harmonics related to the propeller rotation rate.

Insect return.--Swarms of flying insects have long been suspected as one of the causes of radar angels (echoes observed from apparently clear, targetless regions). Attempts to measure individual insect radar cross sections and spectral characteristics of their return have been generally carried out at relatively short wavelengths. However, at least one set of cross-section measurements was performed at both uhf and L band.[10] Table 4 gives empirically determined target

[10] *K. Glover, R. Hardy, T. Konrad, W. N. Sullivan, and A. Michaels, Radar Observations of Insects in Free Flight, Science, 154, 3752 (25 November 1966), 967-972.*

cross sections of three common insects at L band, while at uhf (interestingly enough at 435 MHz--approximately the same frequency as the CDR) the target cross sections were below the minimum detectable cross section. For wavelengths greater than 10 cm, an upper bound on the insect cross section is established by a λ^{-3} relationship.[10] The insect cross sections appearing in table 4 would be diminished by at least an order of magnitude at 435 MHz.

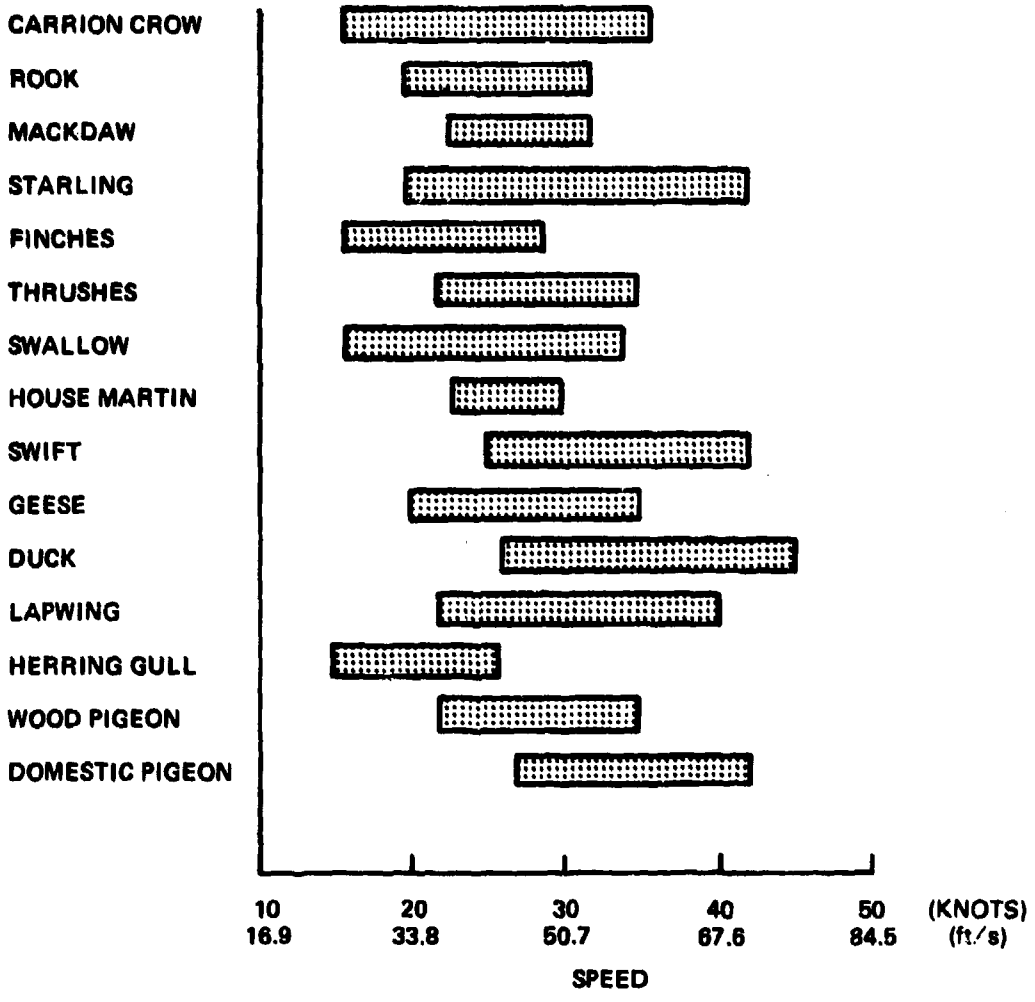

Figure 7. Range of bird velocities (abstracted from ref 7).

[10] K. Glover, R. Hardy, T. Konrad, W. N. Sullivan, and A. Michaels, *Radar Observations of Insects in Free Flight*, Science, 154, 3752 (25 November 1966), 967-972.

TABLE 4. L-BAND RADAR CROSS SECTION OF THREE INSECTS MEASURED IN FREE FLIGHT (ref 10)

Insect target	L-band radar cross section (dBsm)
Wingless Hawkmoth	-60
Honeybee	-63
Dragonfly	-67

Since no studies have been made to determine the statistics of insect return,[7] there is little means of determining whether high enough insect densities will be found at a given geographical location to cause a detection and subsequent track formation.

Because there is motion of the insects within a swarm, the spectral return may not provide a good measure of the swarm's velocity. However, if the fundamental of the wing-beat rate is observed, it could be used to discriminate bird from insect return since insect wing-beat rates are generally higher than bird wing-beat rates. For example, locust wing-beat frequencies range from 14 to 20 Hz, butterflies from 20 to 30 Hz, and crows from only 3 to 4 Hz.

2.1.2 Nontranslating "Target" Return

The power spectral density function of the complex (quadrature) return due to windblown objects such as foliage, power lines, etc, that make no net progress toward the radar, consists of approximately equal positive-frequency and negative-frequency power. In most cases the power spectral density function of the return is nearly symmetrical about 0 Hz.

An empirically determined model that predicts the long-term average power spectral density function for uhf and L-band windblown-foliage backscatter return was previously developed at HDL.[11] A simple exponential was found to describe the data for wind conditions between 2 and 20 mi/hr. The expression for the power spectral density, P(f), is

---

[7] *E. Reedy and T. Cutler, the HOWLS Radar Sky-Clutter Environment, Engineering Experiment Station, Georgia Institute of Technology, ESD-TR-75-319 (15 September 1975).*

[11] *R. Antony, C. Roberts, and S. Peperone, An Investigation of Radar Backscatter from Foliage, 18th Tri-Service Radar Symposium (1972).*

$$P(f) = \begin{cases} S_0 , & 0 < |f| < f_c , \\ S_1 \exp\left(-\beta\sqrt{|f|}\right) , & |f| > f_c , \end{cases} \tag{7}$$

where $S_0 = S_1 \exp\left(-\beta\sqrt{f_c}\right)$, S_1 is an empirically determined constant, and β as a function of wind speed is given in figure 8.

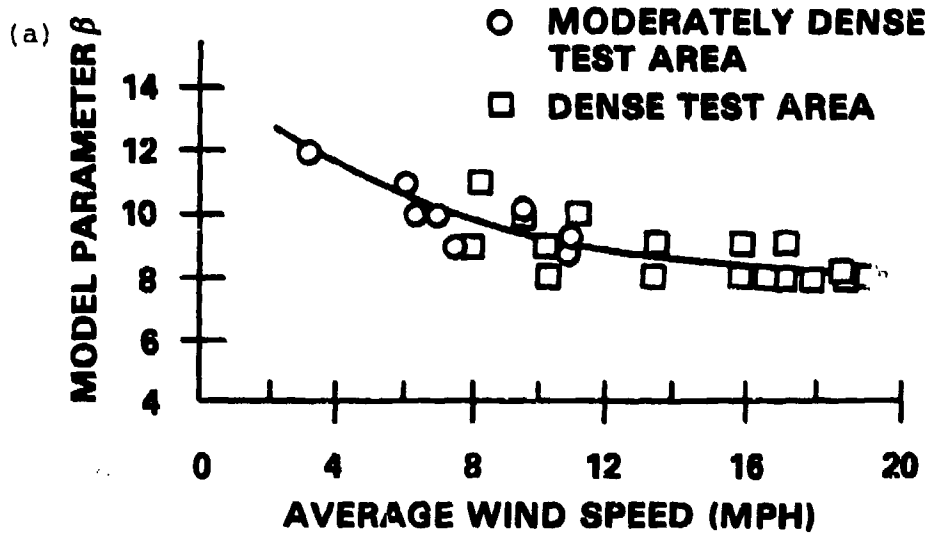

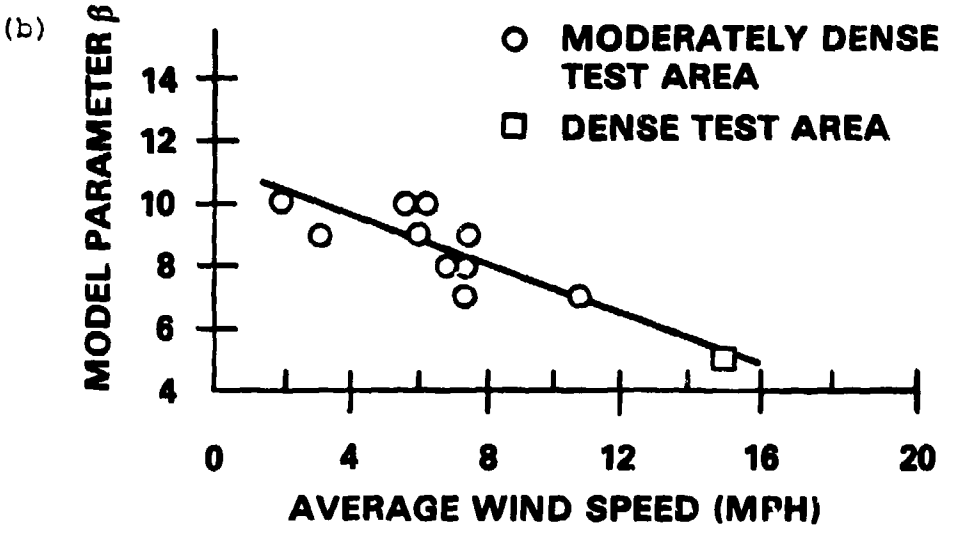

Figure 8. Spectral model parameter β versus average wind speed: (a) UHF, (b) L band (excerpted from ref 11).

2.2 Target Features

The important target characteristics apparent from the translation target model are the measured radial frequency, f_T, and the class-characteristic amplitude modulation, $a_i(t)$, and angle modulation, $\phi_i(t)$. The following six features have been derived from equation (3) and were discussed in the last section as applicable to the various target models:

(a) f_T = target radial translational frequency

(b) f_0 = target natural frequency (e.g., half the step rate, R_0, of a human; wing-beat rate of a bird)

(c) $d_0 = (\lambda f_T/4f_0) \sec \gamma$ (e.g., step size of human, distance of travel in one wing beat of a bird)

(d) n_S = number of harmonics of f_0 observed in the power spectral density function of the return within specified power-level and signal-to-noise ratio constraints

(e) Δf_T = spectral width of the target translational frequency

(f) Δf_0 = spectral width of the fundamental of the target resonant frequency

The feature n_S accounts for the gross nature of the class-characteristic amplitude and angle modulation observed in the return. The feature Δf_T is related to the rate of change of the target translational velocity for straight-line motion. Target acceleration is generally greater for a low-mass target such as a bird than for a relatively high-mass target such as a human. The spectral spreading of the target resonant frequency tends to be a class-dependent characteristic that is useful in high signal-to-noise ratio return.

The values of features are estimated by algorithms that associate the features with the 20 largest distinct peaks of the power spectral density function of the return. Proper classifier performance depends on the correct determination of f_T and f_0. Since a target can be incoming or outgoing, the spectral character of the nontranslating part of the target return is biased by the radial translational frequency so that most, but not all, of the return consists of either positive or negative frequency components. Since the limb motion occurs forward and backward of the torso, the return should have nearly equal power in both the upper and lower sidebands of the translational lobe.

This criterion has been used effectively to select the proper value of f_T even in cases where some spectral sidelobes are an order of magnitude larger than the translational lobe.

The target velocity depends on the product of the target step size, d_0, and the target step rate, R_0. Assuming that the target step size is directly proportional to the target step rate (the faster one walks, the larger the step size), then a "consistency criterion" can be developed to associate the most likely spectral peak with the spectral feature f_0.

2.3 Target Discrimination

Target discrimination as addressed in this paper is based on the classical likelihood ratio for composite hypotheses (parameters that are random variables):

$$\Lambda_{ij} = \frac{\int p(y|\Theta,H_i)\, p(\Theta|H_i)\, d\Theta}{\int p(y|\Theta,H_j)\, p(\Theta|H_j)\, d\Theta} \quad , \tag{8}$$

where Θ is a vector random variable representing the set of target features as discussed in section 2.2, and H_i designates target class i. When an estimate of the feature vector, $\hat{\Theta}$, has been made, the likelihood ratio reduces to

$$\Lambda_{ij} = \frac{p(y|\hat{\Theta},H_i)\, p(\hat{\Theta}|H_i)}{p(y|\hat{\Theta},H_j)\, p(\hat{\Theta}|H_j)} \quad . \tag{9}$$

Applying Bayes' rule, equation (9) can be rewritten in the form

$$\Lambda_{ij} = \frac{p(\hat{\Theta}|y,H_i)\, p(y|H_i)}{p(\hat{\Theta}|y,H_j)\, p(y|H_j)} \tag{10}$$

$$= \frac{p(\Theta|y,H_i)}{p(\Theta|y,H_j)}\, \Lambda_{ij}(y|\hat{\Theta}) \quad , \tag{11}$$

where $\Lambda_{ij}(y|\Theta)$ is the simple hypothesis (fixed parameter) likelihood ratio and $p(\Theta|y,H_i)$ is the a posteriori probability density function (pdf) of the parameter vector conditioned on the target class, evaluated at the estimates of the target features.

The objective is to develop the a posteriori pdf to be evaluated at $\Theta = \hat{\Theta}$. The elements of Θ are defined as the set of spectral features described in the last section:

$$\Theta = (f_T, f_0, n_S, \Delta f_T, \Delta f_0) \quad .$$

For tractability, the joint a posteriori pdf will be approximated by

$$p(\Theta|y,H_i) = p(\Theta_1|y,H_i)\; p(\Theta_2|y,H_i)\; p(\Theta_3|y,H_i) \quad , \tag{12}$$

where

$$\Theta_1 \overset{\Delta}{=} (f_T, f_0, n_S),$$

$$\Theta_2 \overset{\Delta}{=} (f_T, \Delta f_T),$$

$$\Theta_3 \overset{\Delta}{=} (f_0, \Delta f_0), \text{ and}$$

$$p(\Theta_1|y,H_i) \approx p(\hat{f}_T|H_i)\; p(\hat{f}_0|H_i)\; p(\hat{d}_0|H_i)\; p(\hat{n}_S|H_i)\; p(\hat{P}_{sn}|H_i) \quad .$$

The univariate a priori pdf's of the features were developed based on physical constraints, published data, and empirical measurements. The a priori probability $p(d_0|H_i)$ explicitly expresses the dependency between target velocity (i.e., f_T) and target resonant frequency (i.e., f_0). The pdf $p(P_{sn}|H_i)$ relates to the confidence in the spectral feature estimates based on the measured signal-to-noise ratio of the return.

In a similar manner,

$$p(\Theta_2|y,H_i) \approx p\left(\frac{\Delta f_T}{f_T}\middle|H_i\right)$$

and

$$p(\Theta_3|y,H_i) \approx p\left(\frac{\Delta f_T}{f_0}\middle|H_i\right) \quad .$$

As an example, the probability functions of the seven univariate feature density functions for a human target are presented in figure 9. Similar conditional pdf's apply to all other translating target return.

The class-discriminator decision rule is, then, assign the return as due to that class H_i with the largest value of $p(\Theta|y,H_i)$. In general, this represents a nonunique assignment to a target class, since

$p(\theta|y,H_i)$ could be the same for more than one class. An advantage of this decision rule is that it quantifies the likelihood of proper classification and indentifies other target classes possessing nonzero probabilities.

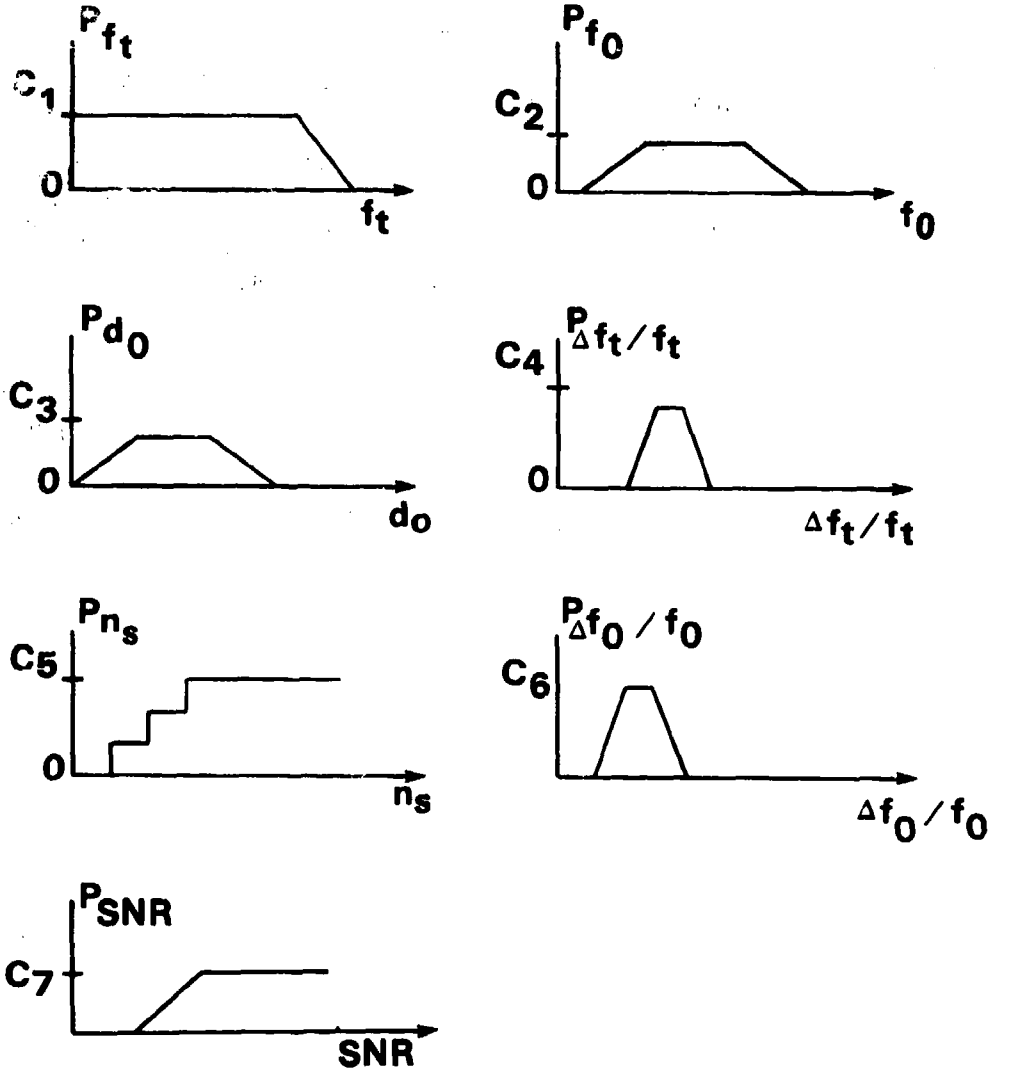

Figure 9. Univariate probability density functions for a human target.

3. CLASSIFICATION RESULTS

3.1 Single-Cell Assessment

The extent of the relatively high signal-to-interference ratio target data base used for classifier design and testing is summarized in table 5. The approximately 330 files of human-target return include data for both single and multiple humans. The single-human return includes walking, jogging, and running targets with various step sizes, step rates, and aspect angles. The multiple-human return includes targets walking in step and out of step, with some carrying M16 rifles. A medium-sized dog (40 lb) was used to obtain the only animal data presently available. A pigeon-sized pheasant was released from within a range-azimuth cell to obtain the bird backscatter data.

Examples of the power spectral density functions of the target return from a radially inbound walking and running human are shown in figures 10 and 11, respectively. An example of an inbound human walking at an angle of 45 degrees relative to radial is shown in figure 12. The power spectral density functions for three inbound humans, an inbound dog, and an inbound vehicle are shown in figures 13 through 15, respectively. Finally, an example of the power spectral density function of the backscatter from wind-blown power lines is shown in figure 16.

TABLE 5. SUMMARY OF ORIGINAL DATA BASE

Target	Number of experiments
Single man (walking, jogging, running)	306
Multiple man (walking, running)	23
Dog	26
Small pheasant	9
Clutter	50
Vehicles	19

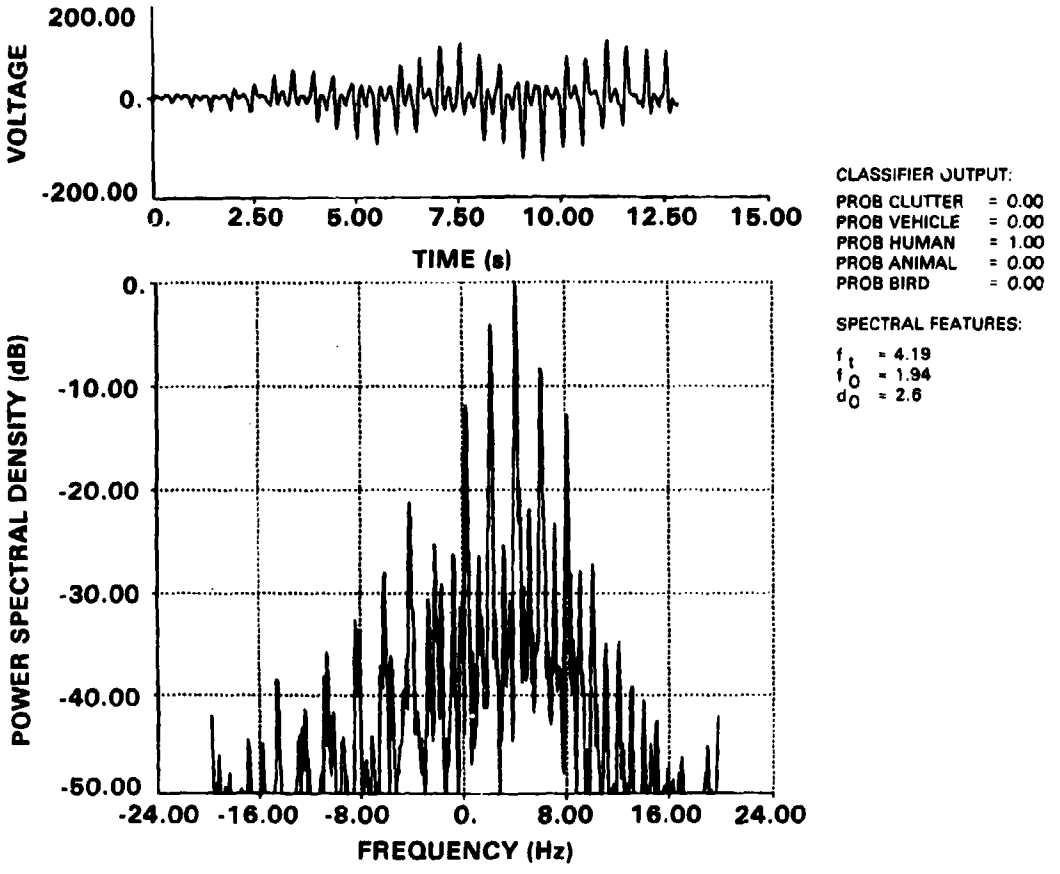

Figure 10. Radar backscatter return from an inbound walking human and corresponding power spectral density function; return was classified as due to a human with probability 1.0.

The performance of a classifier can be expressed in terms of the matrix $[p(H_i|H_j)]$, where $p(H_i|H_j)$ is the probability of choosing hypothesis H_i, given that H_j is true. If this matrix is diagonal, the classification would be ideal. The results of the single-cell assessment using the current target classifiers for the present data base are shown in table 6. For the compilation of these data, the return was classified as due to that target class, H_i, whose probability assessment, $p(\Theta|y,H_i)$, was greater than or equal to 0.5.

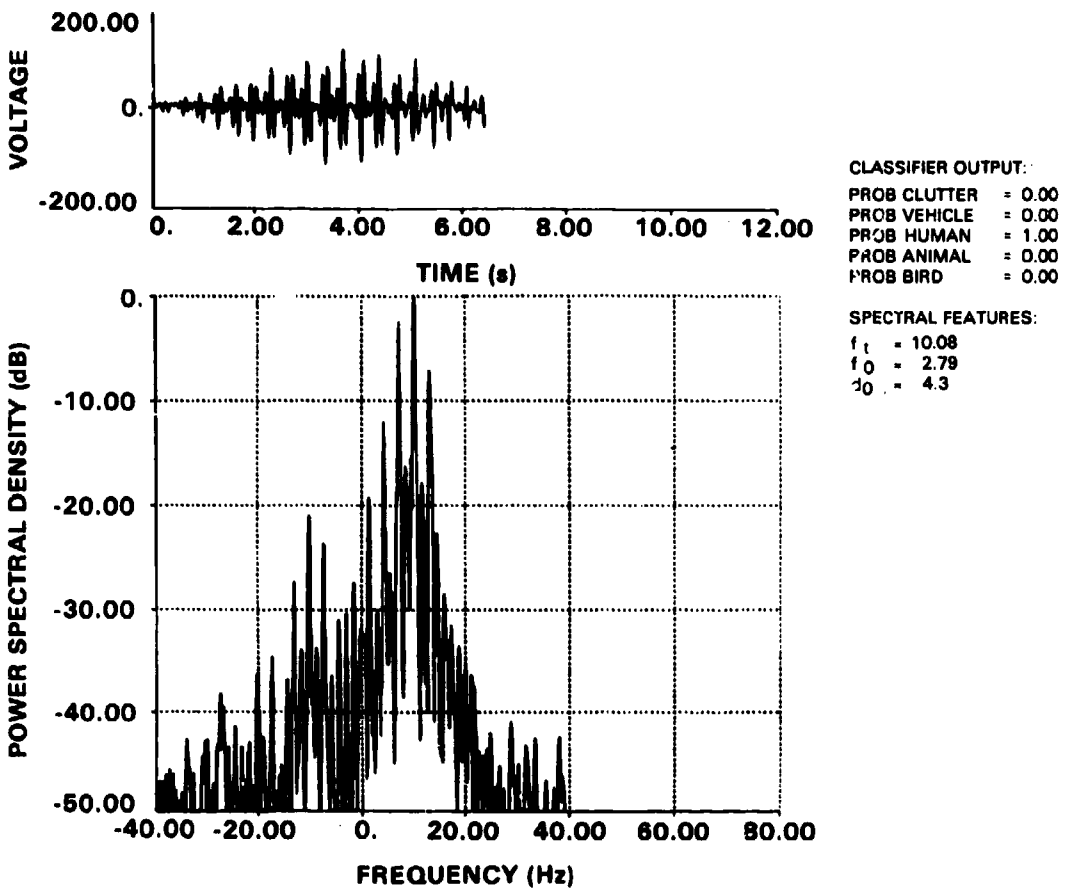

Figure 11. Radar backscatter from an inbound running human and corresponding power spectral density function; return was classified as due to a human with probability 1.0.

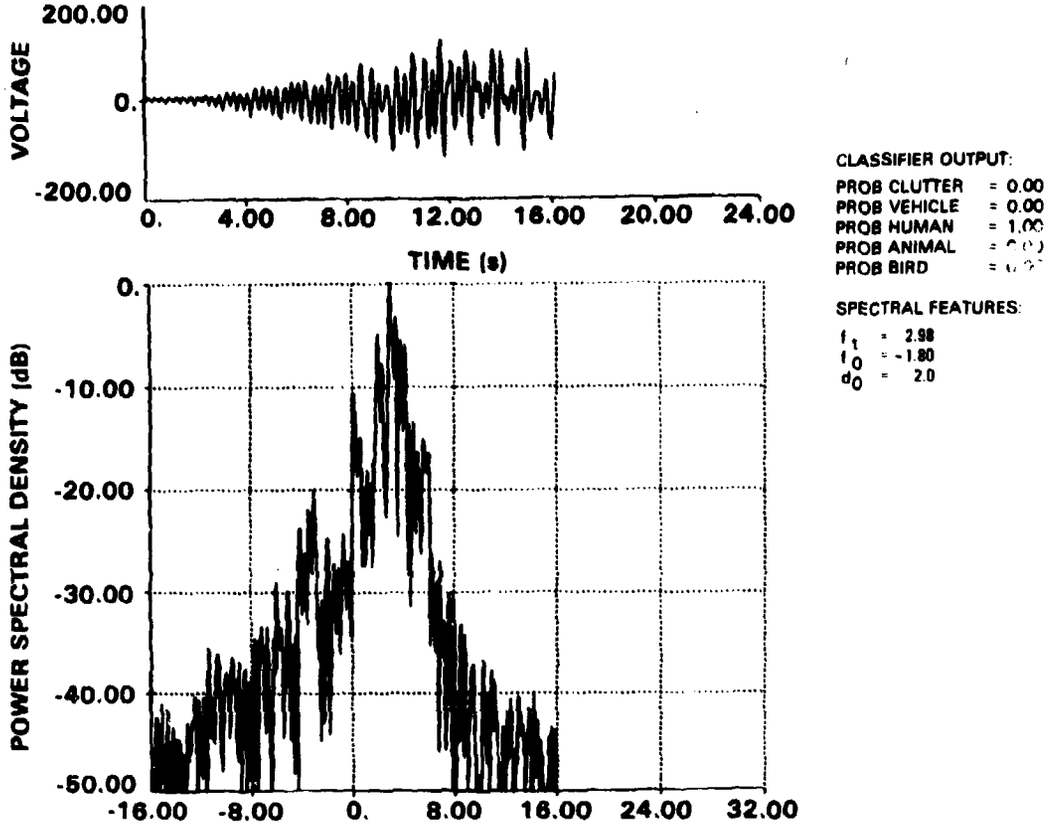

Figure 12. Radar backscatter from an inbound human, walking at a 45° angle relative to radial, and corresponding power spectral density; return was classified as due to a human target with probability 1.0.

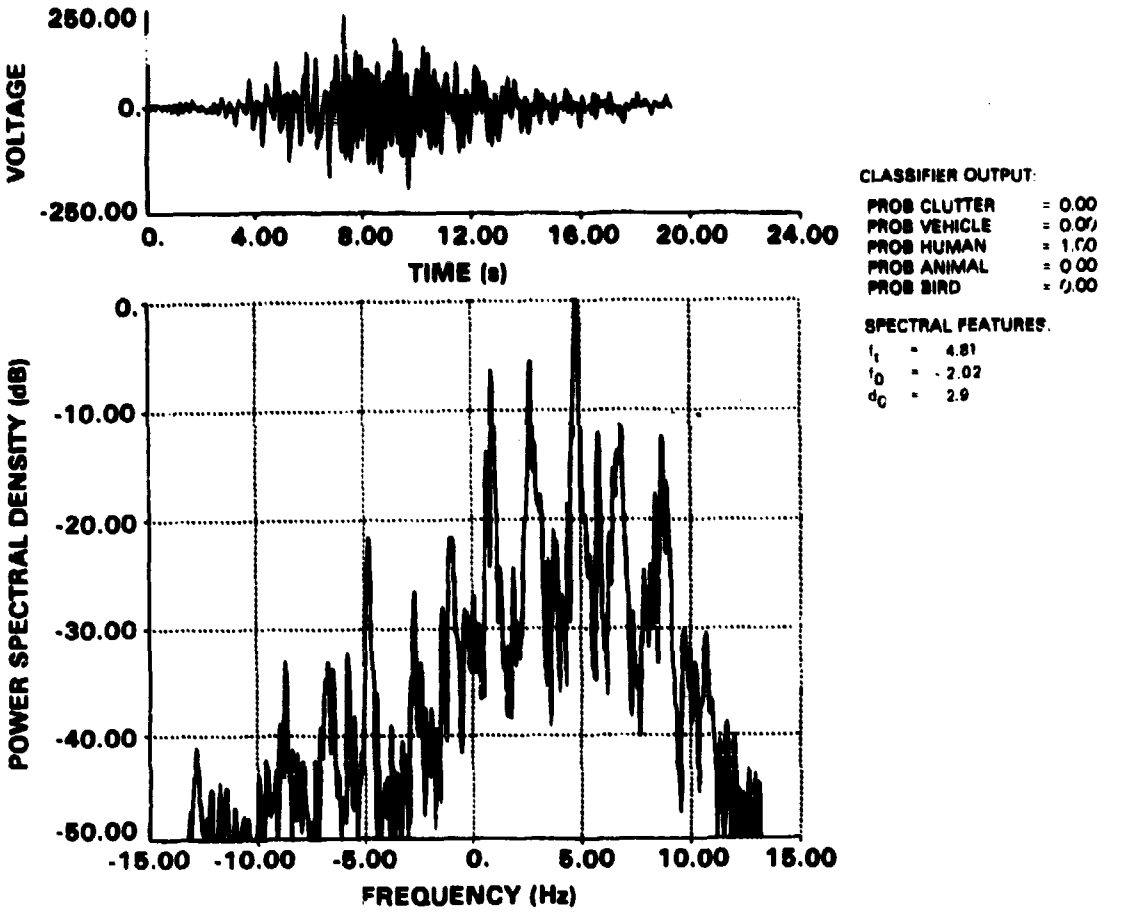

Figure 13. Radar backscatter return from three inbound humans and corresponding power spectral density function; return was correctly classified as due to a human with probability 1.0.

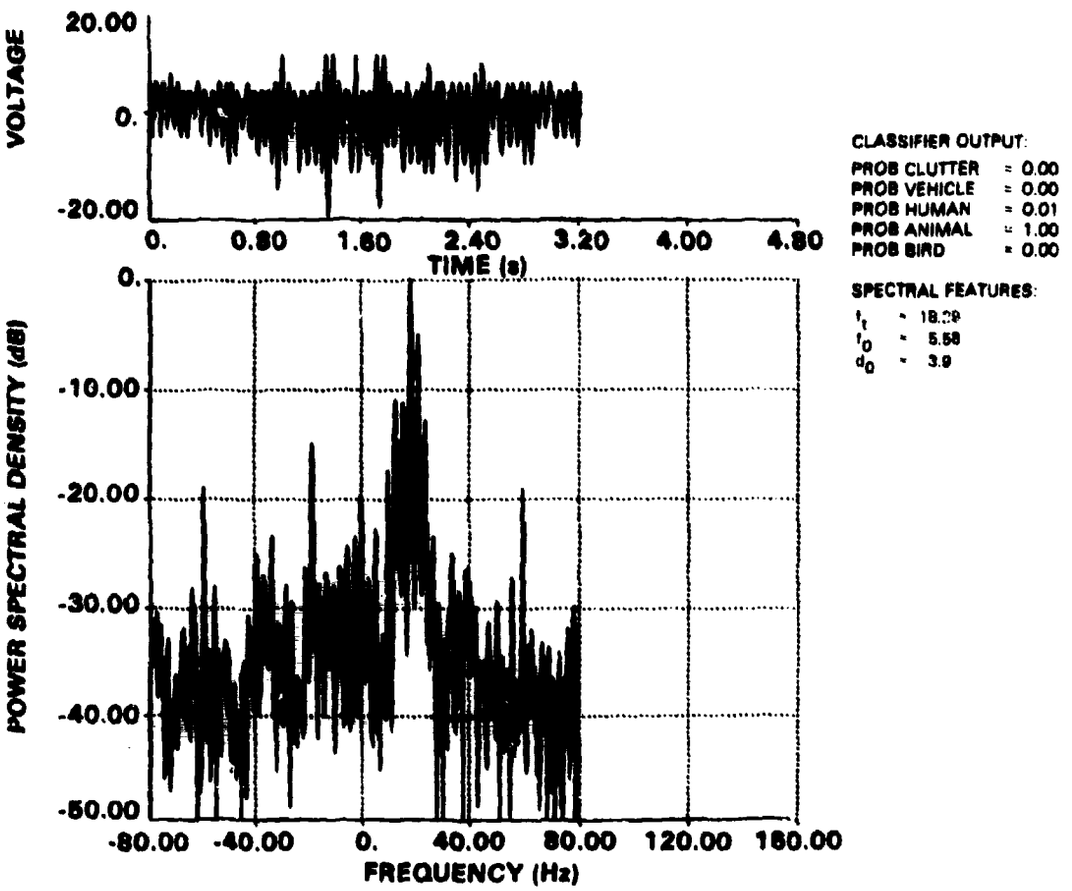

Figure 14. Radar backscatter from a 40-lb dog and corresponding power spectral density function; return was classified as due to an animal with probability 1.0 and as a human with probability 0.01.

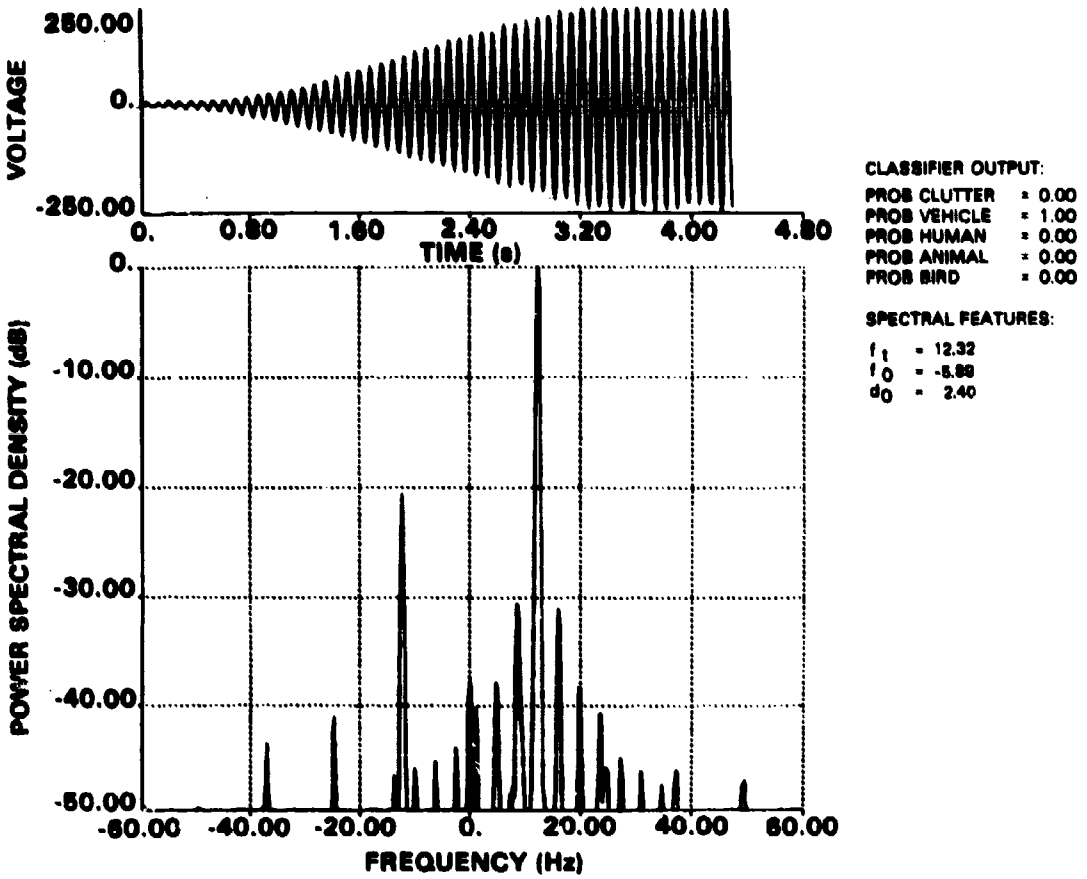

Figure 15. Radar backscatter from an inbound car and corresponding power spectral density function; return was classified as a vehicle with probability 1.0.

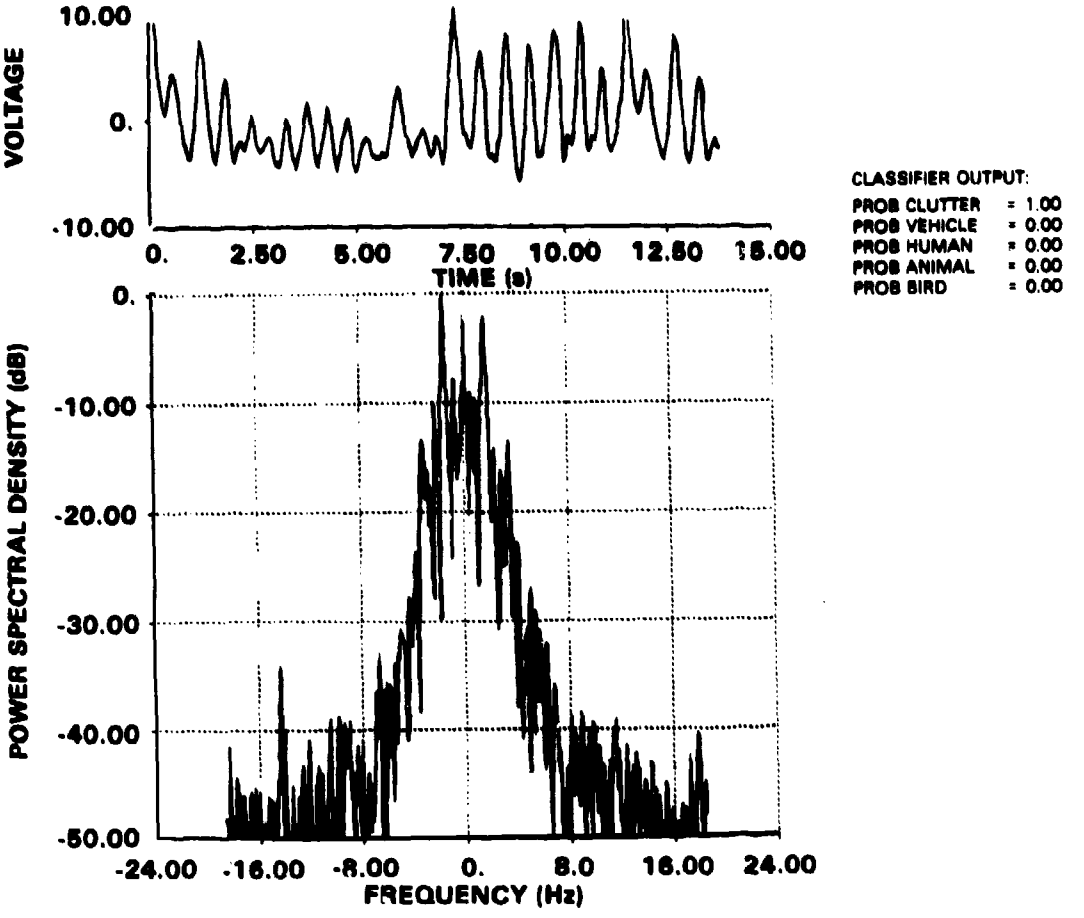

Figure 16. Radar backscatter from windblown power lines and corresponding power spectral density function; return was classified as due to nontranslating target with probability 1.0.

TABLE 6. SINGLE-CELL CLASSIFIER PERFORMANCE SUMMARY

Actual target	Classification				
	Clutter	Vehicle	Human	Animal	Bird
Clutter	1.0	0	0	0	0
Vehicle	0	0.95	0	0.05	0
Single man	0	0	0.92	0.08	0
Multiple men	0	0	0.78	0	0
Dog	0	0	0.04	0.88	0.11
Pheasant	0	0	0	0.11	0.89

For the available data, no nontranslating "target" return was misclassified, nor was any translating target return classified as due to nontranslating return. The probability of a human-target return being properly classified was approximately 92 percent; most of the remaining 8 percent of the human-target return that was not properly classified was from jogging, sprinting, and crouching targets. Approximately 4 percent of the dog return was improperly classified as due to a human. One pheasant return was improperly classified as due to an animal. Nearly 89 percent of the dog return was classified as due to an animal. About 5 percent of the vehicle return and 8 percent of the human return was improperly classified as due to an animal.

3.2 Multiple-Cell Assessment

Although single-cell target classification may not be entirely adequate, as shown in table 6, track classification based on the full track history offers a means of reducing the probability of incorrect target classification.

One possible approach to designing a track classifier is to assume that the single-cell assessments are independent from cell to cell within the track. The statistics collected for the single-cell assessment involve the same targets making repeated passes through a single range gate. The extension from multiple passes through a single cell to a single pass through multiple cells is thus not entirely unreasonable.

Assuming independence from cell to cell, table 7 tabulates the probability of at least L classifications as a human target for a track of length K cells. For instance, approximately 4 percent of the dog return was classified as due to a human target; however, the probability that a target will be classified as a human at least 2 out of 3 times is 98 percent if the target is, in fact, a human and essentially zero if the target is a dog. Similar multiple-cell assessments for classification as an animal or a bird are given in tables 8 and 9. Thus, based on the results of the current classifiers operating on the present data base, high-reliability target assessment for tracks as short as 3 or 4 contiguous cells may be possible.

TABLE 7. PROBABILITY OF AT LEAST L CLASSIFICATIONS AS HUMAN, GIVEN K TOTAL CELLS ASSESSED

Actual target	L = 1 K = 1	L = 1 K = 2	L = 2 K = 3
Human	0.92	0.99	0.98
Dog	0.04	0.08	0.00

TABLE 8. PROBABILITY OF AT LEAST L CLASSIFICATIONS AS ANIMAL, GIVEN K TOTAL CELLS ASSESSED

Actual target	L = 1 K = 1	L = 1 K = 2	L = 2 K = 3
Dog	0.88	0.92	0.96
Pheasant	0.11	0.01	0.00
Human	0.08	0.00	0.00
Vehicle	0.05	0.00	0.00

TABLE 9. PROBABILITY OF AT LEAST L CLASSIFICATIONS AS BIRD, GIVEN K TOTAL CELLS ASSESSED

Actual target	L = 1 K = 1	L = 1 K = 2	L = 2 K = 3	L = 3 K = 4
Bird	0.89	0.99	0.96	0.94
Dog	0.11	0.21	0.03	0.00

A single target may be detected in multiple range-azimuth cells because of range sidelobes, partially overlapping azimuthal antenna patterns, or multipath effects. Although operations such as simple centroiding can be used to reduce these multiple detections to a single range-azimuth cell to be added to the track vector, signature analysis of the return can be used for this purpose. Since the suggested signature processing isolates the target radial velocity component in the spectrum of the return, the probable target location can be assigned to that cell with the largest radial translational component. In addition, the separation of multiple targets with different radial velocities and return with clearly different spectral character is possible before simple centroiding reduces multiple alarming cells to a single alarm.

A historical assessment of the spectral features of the full track history may also provide additional discrimination. A case in point would be for a bird target. While a bird may soar through any given range-azimuth cell on a path nearly tangential to the radar, it may subsequently change to a more radial path and begin beating its wings. Thus, although the initial assessment of the spectrum of the return would yield a poor estimate of the target's actual velocity and no apparent modulation at the species' characteristic wing-beat rate, subsequently the return might be completely characteristic of bird return.

Thus, the overall track assessment could be based on the independent classification assessments from cell to cell within the track and on the statistics of the measured spectral features.

The track assessment, p_{track}, for K total cells assessed might be of the form

$$p_{track}(m) = \frac{\beta_0(m)}{K} \sum_{k=1}^{K} p_k(m) + \sum_{n=1}^{N} \beta_n(m)\, p_\mu(n,m) + \beta'_n(m)\, p_\sigma(n,m) \quad , \tag{13}$$

where

m is the target class (M total classes);

$p_k(m)$ is the probability assessment of the k^{th} cell within the track (k = 1, ..., K);

$p_\mu()$ is the probability assessment for the mean of the n^{th} spectral feature for each target class (n = 1, . . ., N);

$p_\sigma()$ is the probability assessment for the standard deviation of the n^{th} spectral feature for each target class; and

β_0, β_n, β'_n are constants that depend on the target class m.

The track is classified as that target class m with the largest value of $p_{track}(m)$.

For a bird target under track, although several $p_k(\text{bird})$ might be nearly zero if the bird were soaring through these cells, a high standard deviation for the spectral feature f_0 for the entire track, for instance, would be assigned a high value of $p_\sigma(\text{bird})$. The track would be classified as due to a bird target if

$$p_{track}(\text{bird}) \geq p_{track}(m)$$

for all m with associated confidence $p_{track}(\text{bird})$; it would be classified as an unknown target if all $p_{track}(m) < p_{min}$, where p_{min} is a constant. Additional feature statistics such as the minimum and the maximum of a given feature over the entire track history may provide further target discrimination.

An example of the power spectral density function of the return from a wild duck flying through three consecutive range-azimuth cells is shown in figure 17. The bird beats its wings while in range cell No. 1 flying at a radial speed of 42 ft/s, sets its wings in range cell No. 2, and changes direction and soars out of range cell No. 3. This pattern is apparent from both the time series and power spectral density function of the returns. On a single-cell basis, the bird was correctly

classified in range cell No. 1, misclassified as a vehicle in cell No. 2 (because of the lack of a wing-beat modulation), and classified as an unknown target in cell No. 3. Though on a single-cell basis, the return is misclassified in range cells No. 2 and 3, the target track might still be properly classified since such a pattern is characteristic of birds in flight.

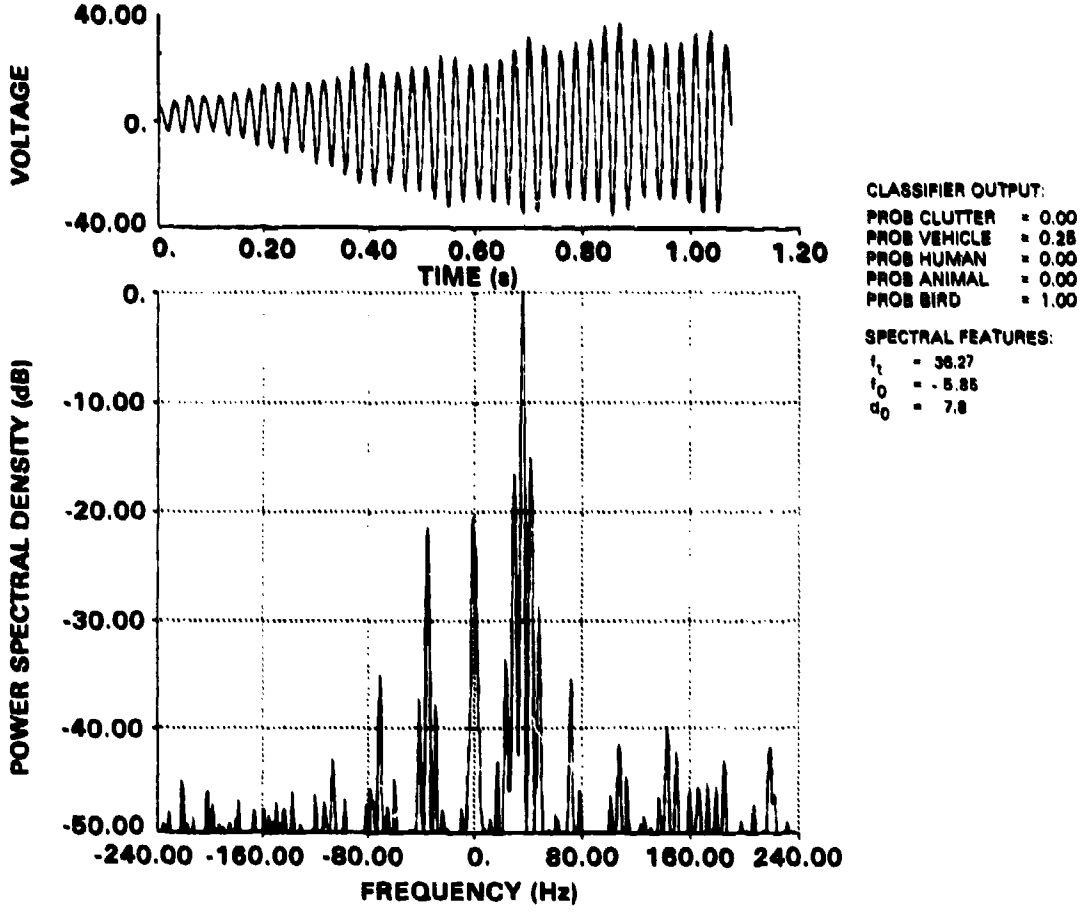

Figure 17. Radar backscatter from a bird passing through three contiguous range-azimuth cells; (a) return was classified as due to a bird in cell 1.

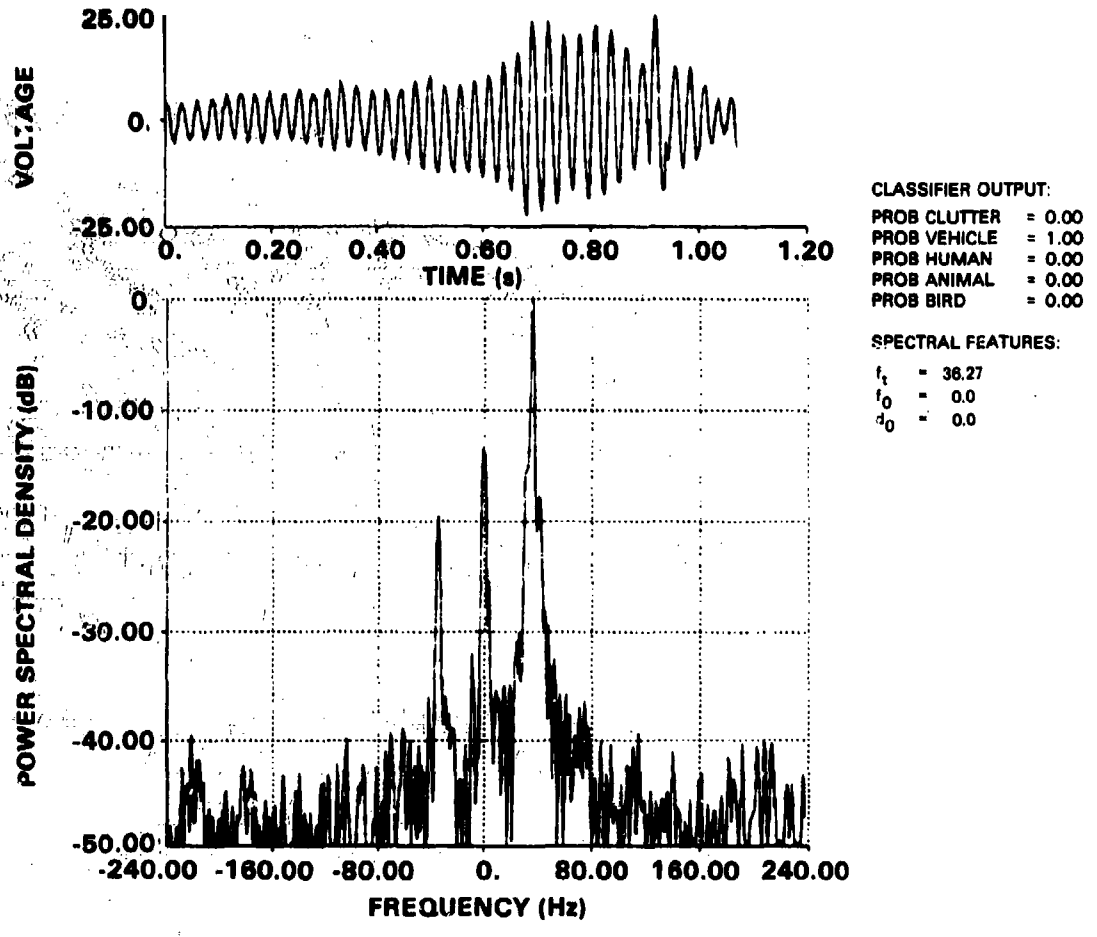

Figure 17 (b). Return was classified as due to a vehicle because of lack of wing-beat harmonics in cell 2.

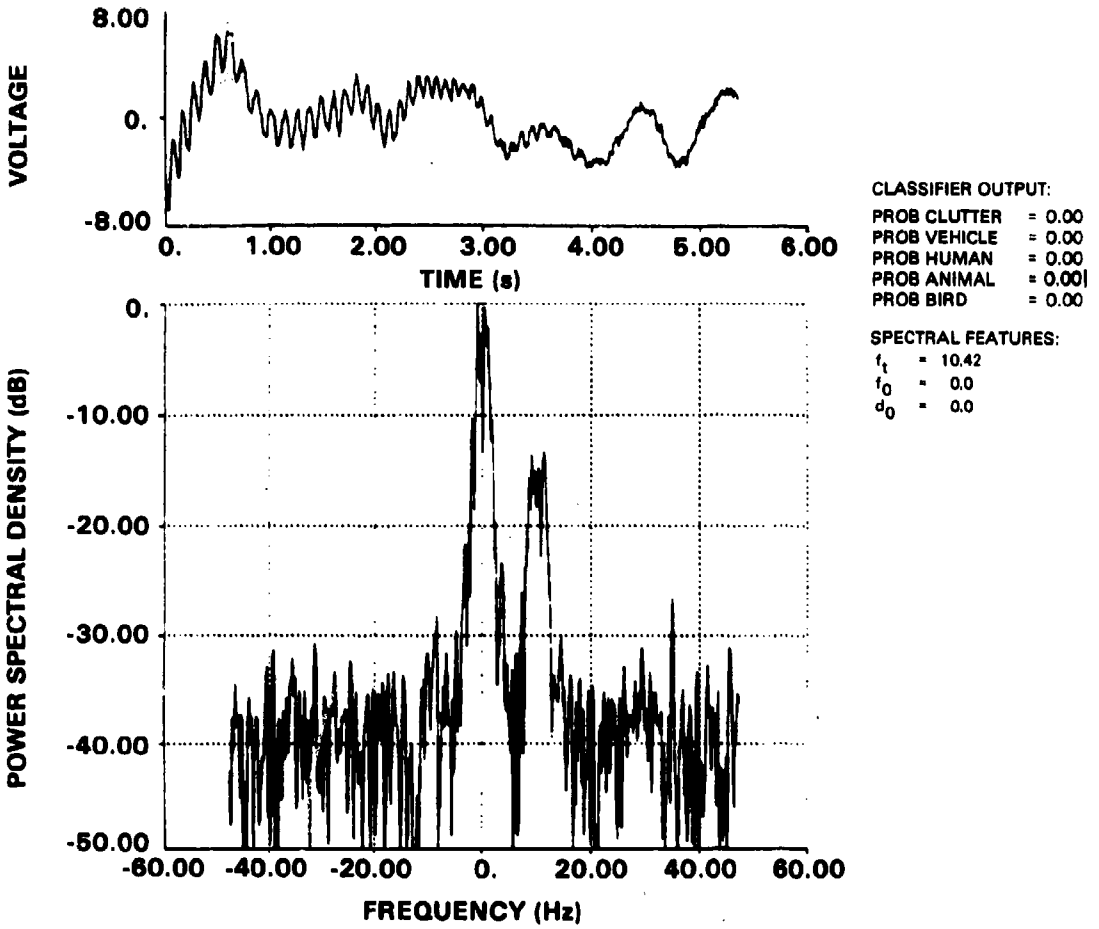

Figure 17 (c). Return was classified as due to an unknown translating target in cell 3.

4. INTEGRATED DETECTION/CLASSIFICATION SYSTEM SIMULATION

A digital simulation of the detection processor has been developed that allows the processing of real radar return on a general-purpose computer. This permits the development of data handling and processing software which will not interfere with the radar hardware. A block diagram of the system interaction is shown in figure 18. The outputs at all stages of processing can be monitored on a graphics display.

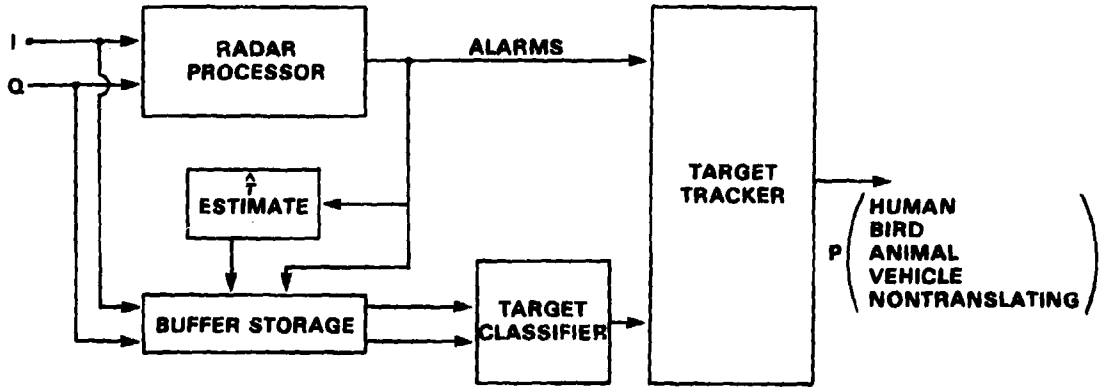

Figure 18. Block diagram of proposed radar system.

When a cell alarm occurs, the raw Doppler return from that cell is collected for the estimated time the target will remain within the range-azimuth cell. An estimate of this interval, $\hat{\tau}$, is selected as

$$\hat{\tau} = \frac{2\alpha\Delta R}{f_R \lambda} \quad , \tag{14}$$

where ΔR is the range cell depth, f_R is the estimated radial translational frequency, the parameter α is a dimensionless quantity that depends on the signal-to-noise ratio and various processor parameters, and λ is the rf wavelength. An estimate of f_R is obtained from the fast Fourier transform of the first 128 samples of the collected data.

Once $\hat{\tau}$ seconds of raw Doppler from an alarming range-azimuth cell have been collected, the data are weighted with a Kaiser-Bessel window and a 512-point discrete Fourier transform (DFT) is computed. The magnitudes of the complex spectral coefficients are calculated and the 20 largest distinct peaks of the resulting estimated power spectral density function are determined. The spectral lobes are then associated with the various spectral features and the target classifiers produce probability assessments for each of the five target classes.

An example of the processor output for a dog passing through a single range-azimuth cell is shown in figure 19. In this case, 5 of the 12 balanced processor channels were monitored. The fixed threshold level was purposely set high so that no threshold crossing occurred.

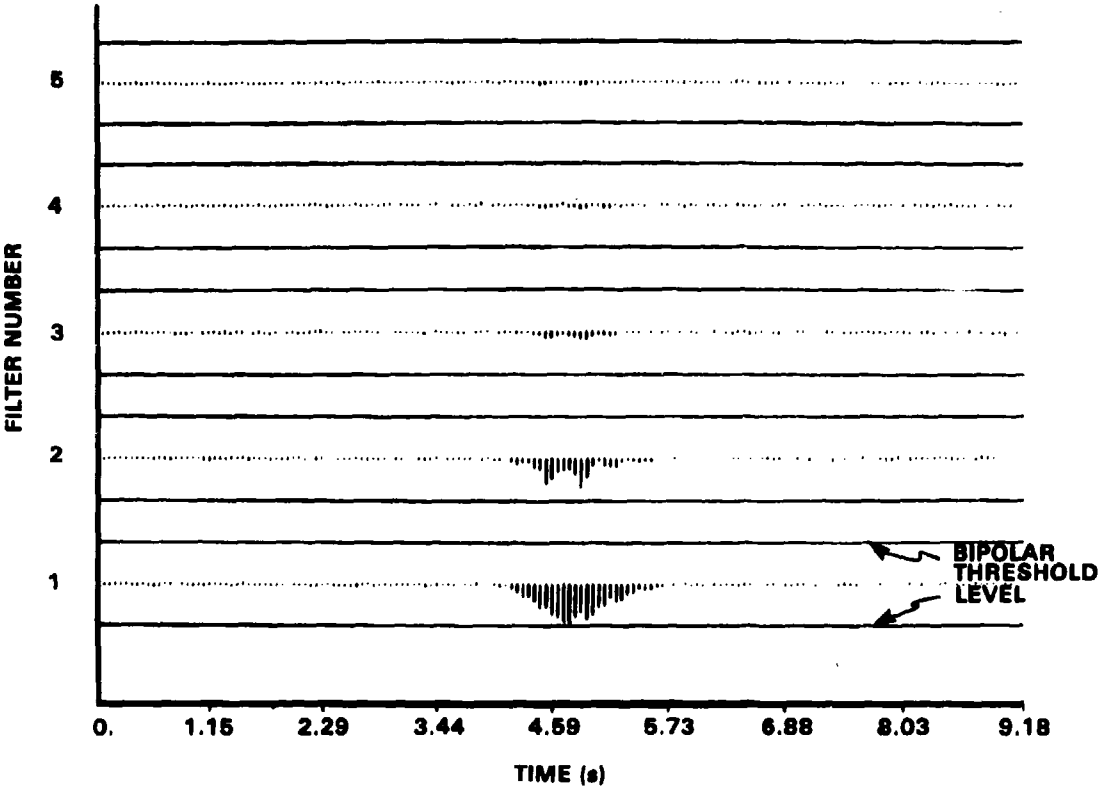

Figure 19. Five of first seven simulated high-velocity filter outputs for a dog target, passing outbound through a single range-azimuth cell; fixed threshold was set so that a threshold crossing would not occur.

In figure 20, the same data are processed using an adaptive constant false-alarm rate threshold level. In this case, detection occurs and the incoming data begin filling a temporary buffer. A 128-point DFT is calculated and a refined estimate of $\hat{\tau}$ is computed. After $\hat{\tau}$ seconds of the Doppler return has been collected, the target classification algorithms are initiated. Figure 21 shows the Doppler waveform of length $\hat{\tau}$ seconds, the corresponding estimate of its power spectral density function, and the classification results. In this case, the detection was assessed as due to an animal target that is outbound with a radial translational frequency of 22.34 Hz and a target natural frequency of 3.27 Hz.

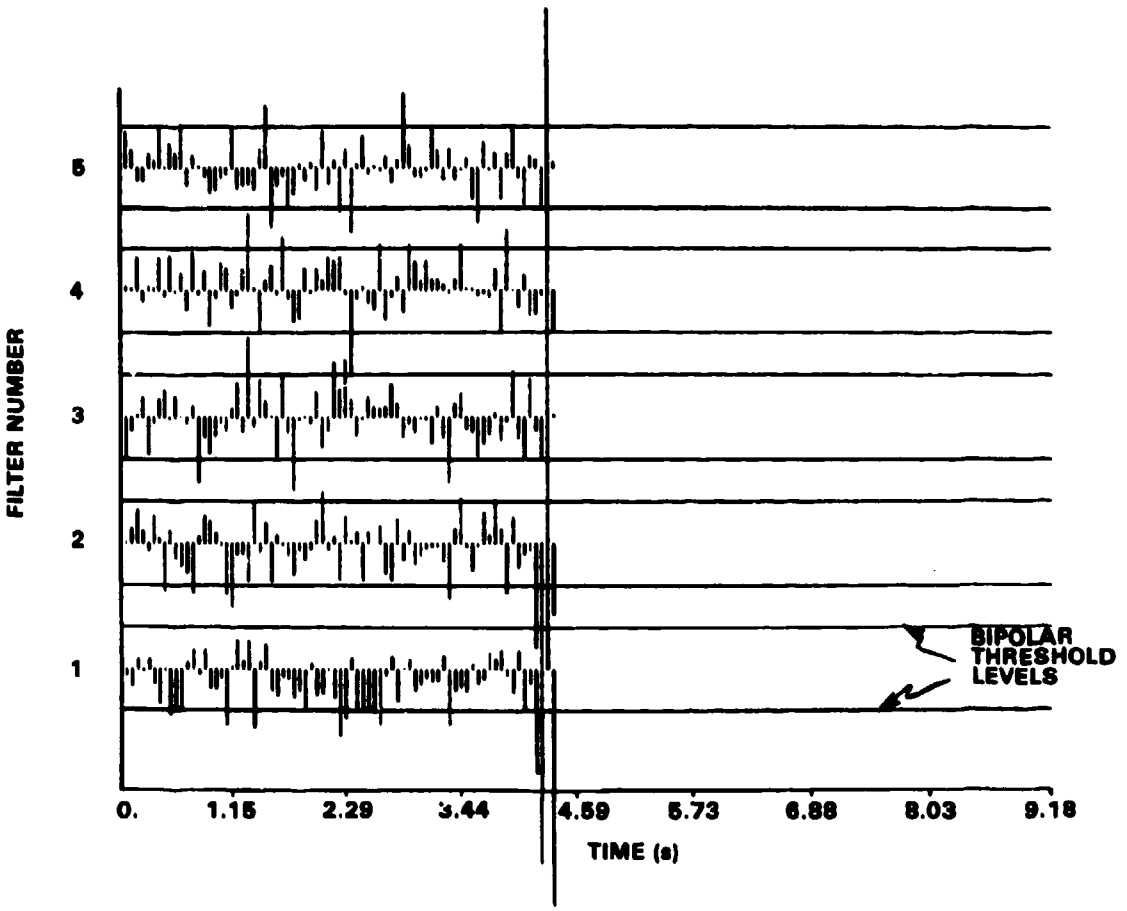

Figure 20. Simulated high-velocity filter outputs for a dog target, passing outbound through a single range-azimuth cell; adaptive threshold was used.

Similar results for both human and bird targets are shown in figures 22 to 26. In all cases, the target classifiers correctly assessed the cause of the processor alarms.

Finally, the processor output for the return from a range-azimuth cell containing no target is shown in figure 27. In this case, the binary integrator output does not cross the threshold and consequently no target detection occurs.

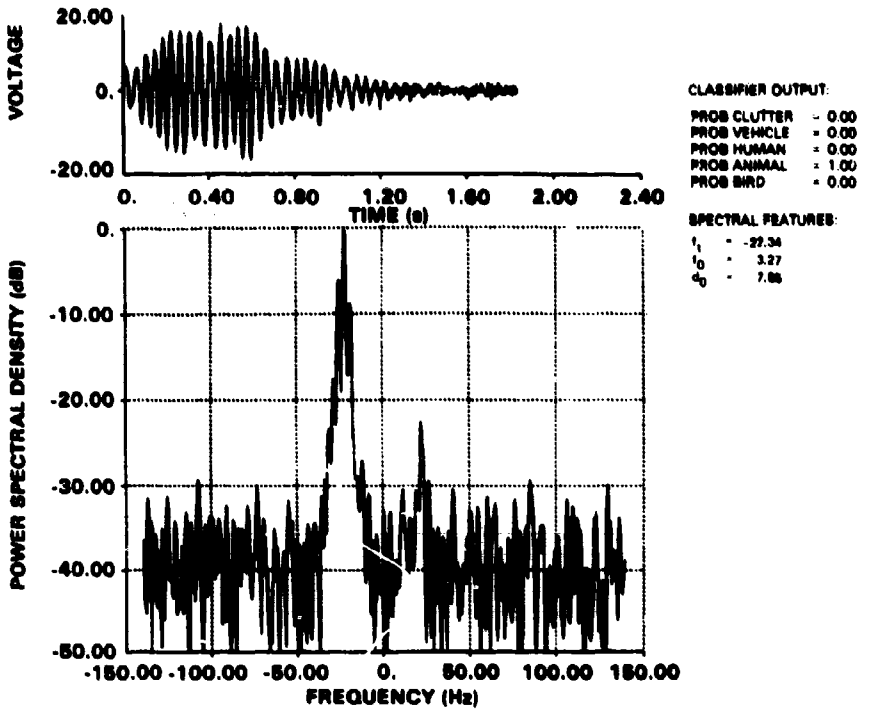

Figure 21. Radar backscatter return from a running dog, collected following target detection indicated in fig. 20; estimated duration of target in range-azimuth cell, $\hat{\tau}$, was calculated to be approximately 1.8 s.

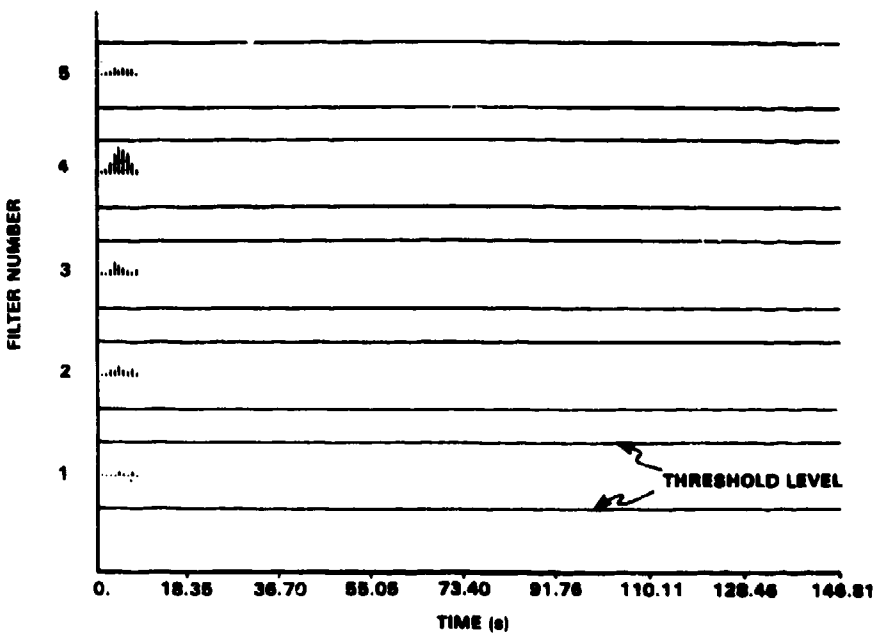

Figure 22. Simulated low-velocity filter outputs for a human passing outbound through a single range-azimuth cell; fixed threshold was set so that a threshold crossing would not occur.

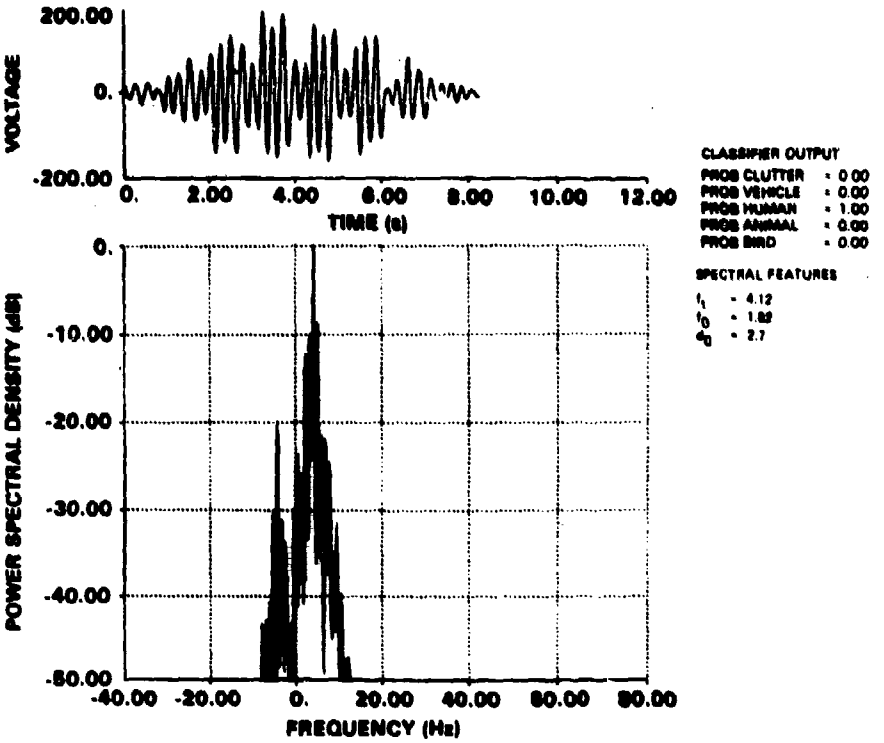

Figure 23. Radar backscatter return from a human target, collected following target detection indicated in fig. 22; estimated duration of target in range-azimuth cell was calculated to be approximately 8 s.

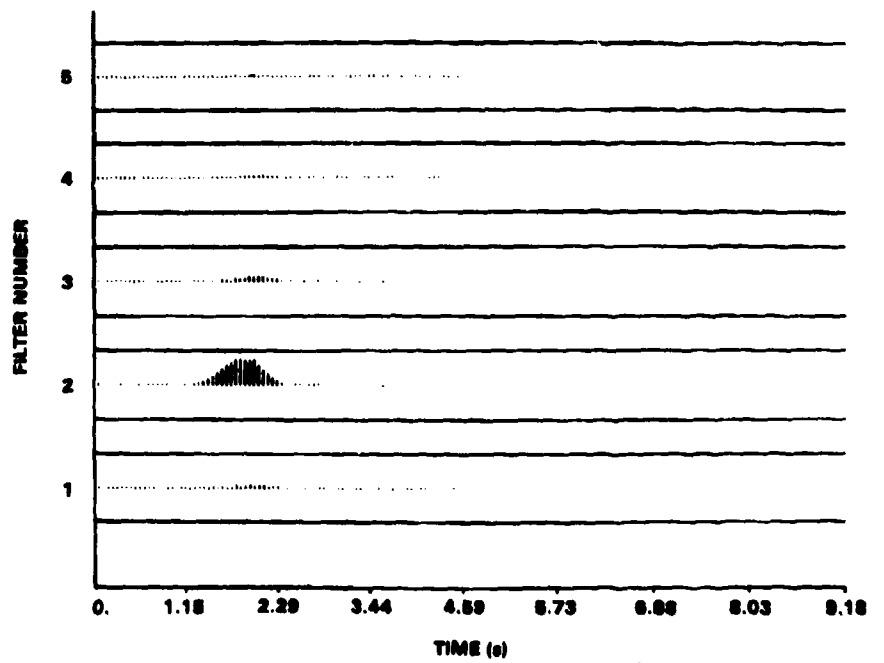

Figure 24. Simulated high-velocity filter outputs for a pheasant flying inbound through a single range-azimuth cell; fixed threshold was set so that a threshold crossing would not occur.

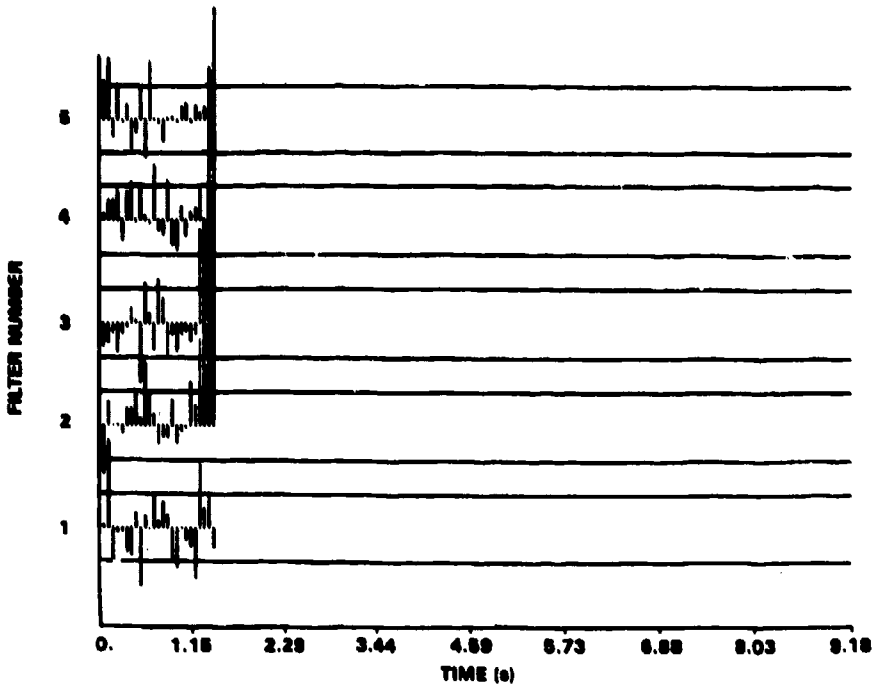

Figure 25. Simulated high-velocity filter outputs for a pheasant flying inbound through a single range-azimuth cell; adaptive threshold was used.

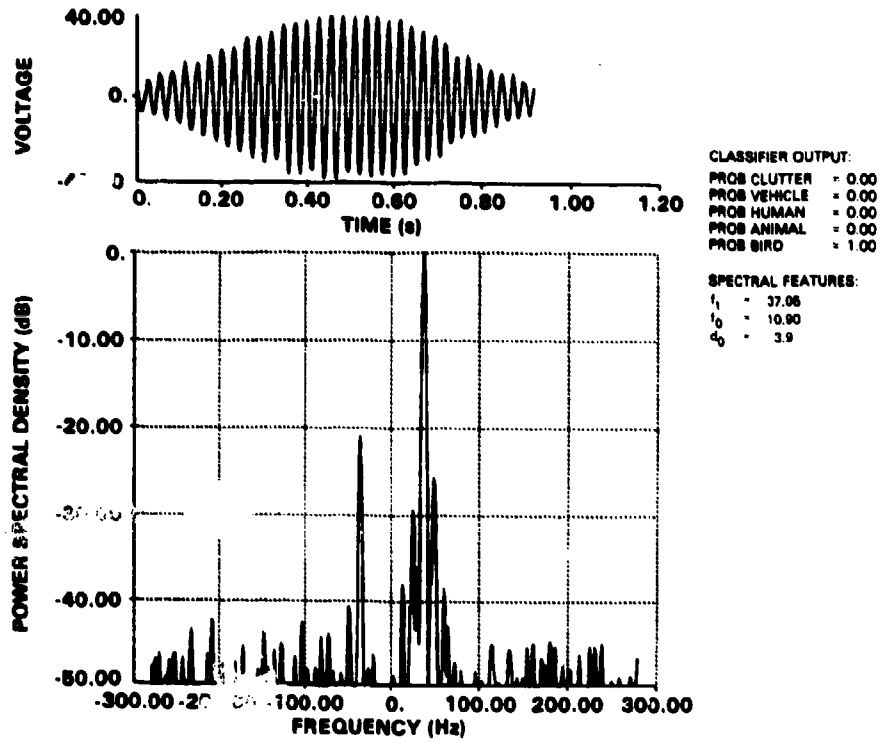

Figure 26. Radar backscatter return from a pheasant, collected following target detection indicated in fig. 25; estimated duration of target in range-azimuth cell was calculated to be approximately 0.9 s.

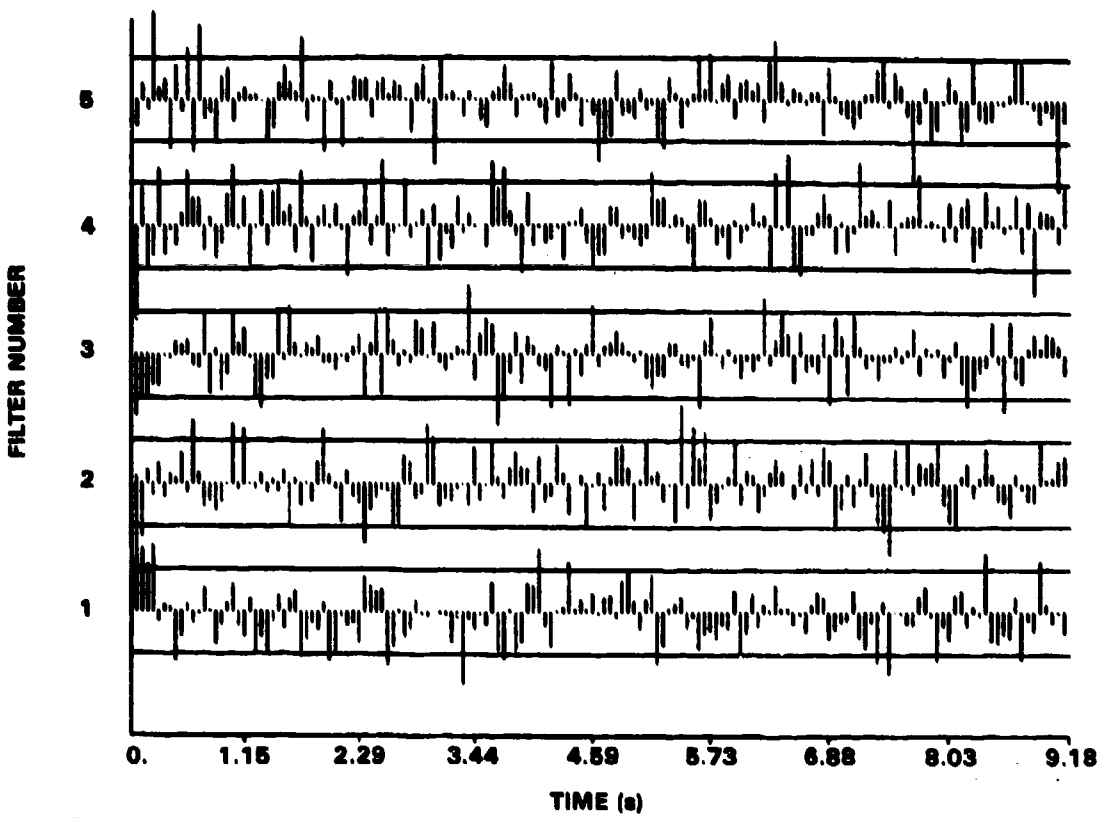

Figure 27. Simulated high-velocity filter outputs for return from a range-azimuth cell not containing any target.

5. SUGGESTIONS FOR FUTURE STUDY

This paper outlines an initial study of a pattern-recognition approach that has rather broad applicability. This section suggests possible extensions of the work that has been discussed here.

Target identification by track classification is essentially a sequential decision problem. As experience is gained with both signature classification and tracking, the current procedures will be refined so that targets can be identified in a minimum time from first detection. Ultimately, the current signature-classification structure may evolve into a sequential classifier where the various features are obtained using recursive estimators. This approach might reduce both the computational and storage requirements of a real-time system.

A fundamental limitation of track classification involves a form of information overload that cannot be circumvented by increased computer speed or memory size. A simple example will suggest the nature of the problem. Let one large bird (large enough to be detected) be released and constrained to fly within a grid of 10 adjacent range cells by 10 adjacent azimuthal cells (100 range-azimuth cells altogether). Even without problems owing to range and azimuthal target spillover, every cell in this grid is likely to alarm within this relatively short period.

Assigning meaningful tracks in this "high target-density environment" (which could certainly be worse) is clearly fraught with problems, quite independent of computer capabilities. Thus, the objective of track assessment must be to eliminate nuisance targets from consideration as rapidly as possible so that a potentially hostile target passing through this grid of cells will be correctly classified and tracked.

Certainly, the classification algorithms should operate efficiently with regard to memory and computational power requirements (e.g., cycle time, parallelism). At least in theory, the estimated spectral features for each cell within a track preserve the essence of the entire track history. Thus, the set of spectral features (or possibly only the recursive feature statistics) and the history of the physical track movement (e.g., closing on a high-value asset) provide a minimal set of data that completely summarizes the track history and yet is efficient in both required memory storage and computational power.

The feature-estimation algorithm discussed in this report involves the use of the DFT in developing the power spectral density function of the target backscatter. An alternative approach that, in general, achieves higher frequency resolution than the DFT method and does not produce the data-weighting function bias inherent in this method is the autoregressive or maximum entropy method. In using this approach, the assumption is that the signal is generated by a finite dimensional process so that the signal spectrum can be expressed by a rational polynomial model.[12]

Because the target return appears to be adequately modelled by a finite-dimensional system as discussed in section 2, any return from the signal classes of interest may lend itself to high-resolution spectral analysis. One of the important aspects of this approach is in obtaining relatively high resolution from short-length records. Bird return tends to become more nonstationary (in the statistical sense) as the record length increases. Thus, more reliable classification of bird targets may be possible using autoregressive spectral estimation of short-length returns.

---

[12] *Proceedings of the RADC Spectrum Estimation Workshop, Rome Air Development Center (May 1978).*

Other areas that need to be addressed in detail during future studies include

(1) splitting and merging tracks and one track overtaking another track,

(2) correct association of targets for crossing trajectories,

(3) "intelligent" centroiding of multiple, adjacent-cell detections involving spatial and frequency-domain assessment of return,

(4) long dwell time required by resting targets,

(5) evasive target tactics,

(6) radar masking,

(7) assignment of track priority,

(8) choice of an operating mode in the event of data or computation overload, and

(9) determination of optimal tracker memory so that initial target classifications at the limit of detection range do not adversely bias future assessments.

The following was excerpted from an article by Laveen Kanal[3] to provide the proper perspective on the admittedly high-risk objective of reliable target classification based on radar backscatter:

"For the most part, however, technique development has occurred without much feedback from experiments, since meaningful experimentation in pattern recognition often requires that significant resources be spent on collection, verification and handling of large data bases ... In many application areas, effective use of the data requires close interaction with persons knowledgeable about the processes that generate the data. Also required is a sustained effort devoted to the particular application."

Although a sustained effort is still required to expand the present data base, refine the current target classifiers, and explore the limitations of the approach, very encouraging results have been obtained to date. This program has had the benefit of a relatively large, high-quality data base, excellent computer and graphics facilities, and close interaction between experimentation and algorithm development.

[3] *L. Kanal, Patterns in Pattern Recognition: 1968-1974, IEEE Trans. Inf. Theory, IT-20, 6 (November 1974), 697-722.*

6. SUMMARY AND CONCLUSIONS

Target-classificaton algorithms have been developed using target modeling in conjunction with a large data base of labeled radar return. At the present time, target classifiers for walking humans, vehicles, dogs, birds, and nontranslating targets have been developed and tested; results have been reported here.

The structural pattern-recognition approach to classifier design seems to be tailored to the nature of radar backscatter from the classes of moving targets considered. No classifier training in the usual sense is required, and thus the entire data base can be used for testing classifier performance. Large computing power is not required for feature selection and ranking. The method results in a very simple classifier implementation involving the fast Fourier transform, simple logic, and arithmetic computations. Additionally, the classifiers can be easily refined as future data become available.

A digital simulation of the radar processor that develops range-azimuth cell alarms was implemented on a general-purpose digital computer. Based on this simulation, a software interface was developed between the detection and target-classification processing. The current results of this study show that relatively simple algorithms appear to be adequate for automating target classification on a single-cell basis. The target tracker would use the single-cell classification assessment for each cell within a target track and the measured feature statistics in assigning an overall track classification.

On a single range-azimuth cell basis, it appears possible to provide reasonably reliable identification of threatening (human and vehicle) targets and nonthreatening (animal, bird, nontranslating) targets. By using track as opposed to single-cell assessment, rather high-confidence-level classification appears to be possible for tracks as short as three or four range-azimuth cells.

ACKNOWLEDGEMENT

The author wishes to thank L. T. James of Sandia Laboratories for his suggestions and technical assistance in developing the classification methodology used in this paper.

LITERATURE CITED

(1) R. Lewis, PMP-2 Processor Handbook, Stein Associates, Inc., Waltham, MA (March 1978).

(2) J. Dent, Camp Sentinel Radar III (U), 18th Tri-Service Radar Symposium (1972). (CONFIDENTIAL)

(3) L. Kanal, Patterns in Pattern Recognition: 1968-1974, IEEE Trans. Inf. Theory, IT-20, 6 (November 1974), 697-722.

(4) M. Skolnik, Introduction to Radar Systems, McGraw-Hill (1980), Ch 12.

(5) G. Pollon, Distribution of Radar Angels, IEEE Trans. Aerosp. Electron. Syst., AFS-8, 6 (November 1972), 721-727.

(6) D. Atlas and K. Hardy, Radar Analysis of the Clear Atmosphere: Angels, Progress in Radio Science 1963-66, International Scientific Radio Union, 15th General Assembly, Munich (5-15 September 1966).

(7) E. Reedy and T. Cutler, The HOWLS Radar Sky-Clutter Environment, Engineering Experiment Station, Georgia Institute of Technology, ESD-TR-75-319 (15 September 1975).

(8) W. Flock and J. Green, The Detection and Identification of Birds in Flight, Using Coherent and Noncoherent Radars, Proc. IEEE, 62, 6 (June 1974), 745-753.

(9) T. Konrad, J. Hicks, and E. Dobson, Radar Characteristics of Birds in Flight, Science, 159, 3812 (January 1968), 274-280.

(10) K. Glover, R. Hardy, T. Konrad, W. N. Sullivan, and A. Michaels, Radar Observations of Insects in Free Flight, Science, 154, 3752 (25 November 1966), 967-972.

(11) R. Antony, C. Roberts, and S. Peperone, An Investigation of Radar Backscatter from Foliage, 18th Tri-Service Radar Symposium (1972).

(12) Proceedings of the RADC Spectrum Estimation Workshop, Rome Air Development Center (May 1978).

APPENDIX A.--RADAR EQUATION FOR PROPAGATION OVER A PERFECTLY REFLECTING GROUND PLANE

In this appendix the radar equation for propagation over a perfectly reflecting ground plane is derived. This analysis follows the work of Skolnik[1] but is adapted to the case of ground surveillance.

The presence of the ground causes a ground-reflected wave that intercepts the target with a different phase than the direct path wave as shown in figure A-1. The radar is assumed to be horizontally polarized; the ground is assumed to be a flat, perfectly reflecting surface with a reflection coefficient of -1.

The difference in path length between the direct wave and the reflected wave, δ, may be easily determined by noting two equalities in the geometrical construction of figure A-1, i.e.,

$$\text{Direct path length} = AT \approx CGT \ , \ R \gg h_a \ , \qquad \text{(A-1)}$$

$$\text{Reflected path length} = AGT = BGT \ .$$

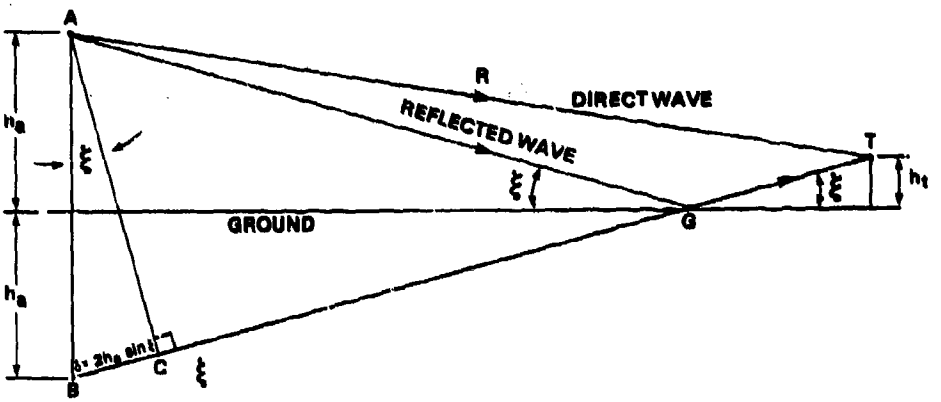

Figure A-1. Geometrical construction for determining phase differential between direct and ground-reflected waves for a target above a perfectly reflecting ground plane.

---

[1] M. Skolnik, *Introduction to Radar Systems*, McGraw-Hill (1980), Ch 12.

Thus,

$$\delta \triangleq AGY - AT \approx BGT - CGT = 2h_a \sin \xi \quad . \tag{A-2}$$

Now, since

$$\frac{GT}{h_t} = \frac{AG}{h_a} \quad , \tag{A-3}$$

$$R = AT \quad , \tag{A-4}$$

and

$$\sin \xi = \frac{h_t}{GT} \quad , \tag{A-5}$$

it then follows that

$$\sin \xi = \frac{h_t + h_a}{R} \quad , \tag{A-6}$$

or

$$\xi \approx \frac{h_t + h_a}{R} \quad ,$$

for small ξ. Therefore,

$$\delta = 2h_a \left(\frac{h_t + h_a}{R} \right) \quad . \tag{A-7}$$

The phase difference, ψ_d, between the ground-reflected and direct waves is then $\psi_d = 2\pi\delta/\lambda$; the total phase difference, ψ, between the two paths is

$$\psi = \psi_d + \pi \quad .$$

At the target, the resultant power of two signals with unit amplitude but with phase difference ψ is

$$2(1 + \cos \psi) = 4 \sin^2 \left(\frac{\psi_d}{2} \right) \quad . \tag{A-8}$$

Defining β as the field strength at the target in the presence of a ground plane relative to the field strength at the target in free space, the power reradiated back to the radar via the direct and reflected paths is proportional to

$$\beta^4 = 16 \sin^4 \frac{\psi_d}{2} = 16 \sin^4 \left[\frac{2\pi h_a (h_t + h_a)}{\lambda R}\right] . \quad \text{(A-9)}$$

The radar equation is then scaled by β^4, the propagation factor, thus:

$$\frac{P_R}{P_T} = \frac{G^2 \lambda^2 \sigma_t}{(4\pi)^3 R^4} \beta^4 = \frac{16 G^2 \lambda^2 \sigma_t}{(4\pi)^3 R^4} \sin^4 \left[\frac{2\pi h_a (h_t + h_a)}{\lambda R}\right] . \quad \text{(A-10)}$$

When ψ_d is small, the radar equation becomes

$$\frac{P_R}{P_T} = \frac{4\pi G^2 \sigma_t}{\lambda^2 R^8} H , \quad \text{(A-11)}$$

where

$$H \triangleq h_a^4 (h_t + h_a)^4 .$$

The presence of the ground plane causes the elevation coverage to break up into the lobed pattern given by equation (A-10).

The first maximum of the antenna pattern occurs when

$$4 \frac{h_a (h_t + h_a)}{\lambda R} = 1 .$$

This first lobe will occur closer to the ground if the antenna height, h_a, is made larger.

DISTRIBUTION

ADMINISTRATOR
DEFENSE TECHNICAL INFORMATION
CENTER
ATTN DTIC-DDA (12 COPIES)
CAMERON STATION, BUILDING 5
ALEXANDRIA, VA 22314

COMMANDER
US ARMY RSCH & STD GP (EUR)
ATTN CHIEF, PHYSICS & MATH BRANCH
FPO NEW YORK 09510

COMMANDER
US ARMY ARMAMENT MATERIEL
READINESS COMMAND
ATTN DRSAR-LEP-L, TECH LIBRARY
ROCK ISLAND, IL 61299

COMMANDER
US ARMY MISSILE & MUNITIONS
CENTER & SCHOOL
ATTN ATSK-CTD-F
REDSTONE ARSENAL, AL 35809

DIRECTOR
US ARMY MATERIEL SYSTEMS ANALYSIS
ACTIVITY
ATTN DRXSY-MP
ABERDEEN PROVING GROUND, MD 21005

DIRECTOR
US ARMY BALLISTIC RESEARCH LABORATORY
ATTN DRDAR-TSB-S (STINFO)
ABERDEEN PROVING GROUND, MD 21005

US ARMY ELECTRONICS TECHNOLOGY
& DEVICES LABORATORY
ATTN DELET-DD
FT MONMOUTH, NJ 07703

HQ, USAF/SAMI
WASHINGTON, DC 20330

TELEDYNE BROWN ENGINEERING
CUMMINGS RESEARCH PARK
ATTN DR. MELVIN L. PRICE, MS-44
HUNTSVILLE, AL 35807

ENGINEERING SOCIETIES LIBRARY
ATTN ACQUISITIONS DEPARTMENT
345 EAST 47TH STREET
NEW YORK, NY 10017

PROJECT OFFICER
PHYSICAL SECURITY EQUIPMENT
7500 BACKLICK ROAD
SPRINGFIELD, VA 22150

COMMANDER
US ARMY MERADCOM
ATTN DRDME-ZPS
COL R. K. CORNELL
FT BELVOIR, VA 22060

DIRECTORATE OF COMBAT DEVELOPMENTS
ATTN ATZN-MP-CM
MAJ HARRY HIXON
FT MCCLELLAN, AL 36205

US ARMY MILITARY POLICE SCHOOL
TRAINING CENTER
ATTN ATZN-CDM-CE
FT MCCLELLAN, AL 36205

HEADQUARTERS
US ARMY TRAINING & DOCTRINE
COMMAND
ATTN ATCD-S-A
FT MONROE, VA 23651

COMMANDER
US ARMY MOBILITY EQUIPMENT
RESEARCH & DEV COMMAND
ATTN DRDME-X-XI
FT BELVOIR, VA 22060

NAVAL COASTAL SYSTEM CTR
CODE 770S
ATTN JACK C. GRACE
PANAMA CITY, FL 34407

COMMANDER
RADC/OCDE
ATTN LEONARD STRAUSS
GRIFFISS AFB, NY 13441

HEADQUARTERS
ATTN ROBERT O'NEIL, JR.
ATTN ESD/OCB
HANSCOM AIR FORCE BASE
BEDFORD, MA 01731

DYNATREND INC.
ATTN E. E. HAMILTON
21 CABOT ROAD
WOBURN, MA 01801

GEORGIA INSTITUTE OF TECHNOLOGY
RADAR & INSTRUMENTATION LAB
ATTN NICHOLAS C. CURRIE
ATLANTA, GA 30332

LOS ALAMOS SCIENTIFIC LAB
OS-DO MS677
ATTN J. F. MCCLARY
LOS ALAMOS, NM 87545

MASON & HANGER
SILAS MASON CO., INC
PANTEX PLANT
ATTN DOSS LEDBETTER
ST. FRANCIS, TX 79069

SANDIA LABORATORIES
ATTN JOHN KANE
DIVISION 1766
ALBUQUERQUE, NM 87115

US ARMY ELECTRONICS RESEARCH
& DEVELOPMENT COMMAND
ATTN TECHNICAL DIRECTOR, DRDEL-CT

HARRY DIAMOND LABORATORIES
ATTN CO/TD/TSO/DIVISION DIRECTORS
ATTN RECORD COPY, 81200
ATTN HDL LIBRARY, 81100 (2 COPIES)
ATTN HDL LIBRARY, 81100 (WOODBRIDGE)
ATTN TECHNICAL REPORTS BRANCH, 81300
ATTN LEGAL OFFICE, 97000
ATTN CHAIRMAN, EDITORIAL COMMITTEE
ATTN R. E. MORRISON, 13500 (GIDEP)
ATTN D. L. RODKEY, 36100 (2 COPIES)
ATTN E. R. SEBOL, 36200
ATTN J. E. TUTTLE, 21400
ATTN R. FEMENIAS, 21100
ATTN J. S. KRUGER, 15400
ATTN J. D. WEDEL, 15400
ATTN R. P. CHASE, 15300
ATTN G. CIRINCIONE, 15300
ATTN D. GIGLIO, 15300
ATTN B. MULLIGAN, 15300
ATTN J. S. SHREVE, 15300
ATTN V. LEWIS, 15200
ATTN K. H. SANN, 15000
ATTN J. F. SELTZER, 11400
ATTN J. SALERNO, 10000
ATTN R. ANTONY, 15200 (30 COPIES)